

# Double pion photoproduction on nucleon and deuteron

A. Fix and H. Arenhövel

*Institut für Kernphysik, Johannes Gutenberg-Universität Mainz, D-55099 Mainz, Germany*

(Dated: September 6, 2018)

Photoproduction of two pions on nucleon and deuteron is studied for photon energies from threshold up to  $E_\gamma = 1.5$  GeV. For the elementary operator an effective Lagrangean approach is used with resonance and Born contributions. The model parameters are fixed by resonance decay widths and multipole analyses of single pion photoproduction. A satisfactory description of total cross sections of two-pion production on the proton for various charge channels is achieved, except for  $\pi^0\pi^0$  production for which a significant underestimation is found near threshold. The operator then serves for the evaluation of this reaction on the deuteron in the impulse approximation. In addition,  $NN$  rescattering in the final state is taken into account, but  $\pi N$  and  $\pi\pi$  rescatterings are neglected. Results are presented for total cross sections and target asymmetries.

PACS numbers: 13.60.-r, 13.60.Le, 21.45.+v, 25.20.-x

## I. INTRODUCTION

Double pion photoproduction is another important tool for our understanding of nucleon structure besides single pion production. It is usually considered as a complementary reaction serving as the main source of information which can not be obtained otherwise, e.g. from single pion photoproduction. In particular, this process is quite promising for the study of the so-called “missing” resonances which are only weakly coupled to the  $\pi N$  channel [1].

The elementary reaction  $\gamma N \rightarrow \pi\pi N$  is clearly much more complicated than single pion photoproduction. This fact is reflected in the existing theoretical approaches which show a strong model dependence of the results [2, 3, 4, 5]. Among the reasons for this model dependence, we firstly would like to note that the Born amplitude, which is considerably more important than it is in single pion production, has a very complicated structure. Another reason lies in the presence of various interactions between the final particles (FSI). This problem is not present in elementary single pion photoproduction because  $\pi N$  rescattering is already included in the elementary amplitude. So far the most advanced investigation of FSI was performed within the WKB model [6] using as an essential ingredient the dominance of meson exchange in the production mechanism at high energies. It produces quite a strong absorptive effect, which changes dramatically the energy dependence of the cross section. An essentially different approach was realized in [5] where the  $\pi NN$  interaction was reduced to resonance excitations in the quasi two-body  $\pi\Delta$  and  $\rho N$  systems. In contrast to the WKB results, the last method predicts quite an insignificant role of FSI. These difficulties are among others the main reason why the mechanisms of the elementary double pion photoproduction so far appear only partially understood.

The analysis of the various theoretical approaches is usually focused on the experimentally favorable case where the target is a proton, whereas the results on the neutron depend on the model assumptions used for extracting the data from measurements on the deuteron or on other light nuclei. The neutron data are obviously needed for a systematic analysis of the isotopic spin structure of the elementary amplitude. The main question arising in this connection is, what is the role of the “nuclear effects”, e.g., Fermi motion, final state interaction, and two-nucleon production contributions, which prevent a model independent study of the neutron amplitude. Whereas the Fermi motion is naturally included in the spectator model, the interaction between the final particles requires considerably more calculational efforts.

Corrections to the mere quasi free production were partially considered in [7]. It was shown that the experimental yields for  $\pi^+\pi^-$  photoproduction were almost the same for  $^1\text{H}$  and  $^2\text{H}$  targets, so that the total effect from higher order processes in the latter case was expected to be insignificant. The strong validity of the spectator model was also assumed in [8] for the extraction of the  $\gamma n \rightarrow \pi^0\pi^0 n$  cross section. In fact, it is often concluded that FSI and other higher order processes have an insignificant influence simply on the grounds of a good agreement between the data and the impulse approximation. However, such a conclusion is not stringent and might be misleading. Therefore, it is the aim of the present work to study the role of FSI using a refined phenomenological model for the basic elementary amplitude and including in addition the final  $NN$  interaction.

Accordingly, the paper is divided into two parts. The first one is devoted to the elementary reaction while the second deals with purely nuclear effects in the reaction on a deuteron. In Sect. 2 we describe briefly our  $\gamma N \rightarrow \pi\pi N$  model. The emphasis lies on those points, where our approach differs from previous work [2, 3, 4, 5]. The  $\pi\pi$  photoproduction on the deuteron is considered in Sect. 3 where the results are presented and discussed. In several

appendices we describe in detail the formal ingredients of the elementary production operator.

## II. THE $\gamma N \rightarrow \pi\pi N$ MODEL

In this section we will outline the formalism for the photoproduction of two pions on the nucleon

$$\gamma(k, \vec{\epsilon}_\lambda) + N(p_i) \rightarrow \pi^{\mu_1}(q_1) + \pi^{\mu_2}(q_2) + N(p_f), \quad (1)$$

where the 4-momenta of the participating particles, incoming photon, initial and final nucleon and the two pions, are respectively denoted by

$$k = (\omega_\gamma, \vec{k}), p_{i/f} = (E_i, \vec{p}_{i/f}), q_{1/2} = (\omega_{1/2}, \vec{q}_{1/2}). \quad (2)$$

The circular polarization vector of the photon is described by  $\vec{\epsilon}_\lambda$  with  $\lambda = \pm 1$  and the superscript  $\mu_i = 0, \pm 1$  in (1) denotes the charge of the  $i$ th pion.

Using standard covariant normalization for the free particle states [9], the unpolarized differential cross section in the overall c.m. frame can be expressed in terms of the reaction matrix  $t_\lambda^{\mu_1\mu_2}$

$$d\sigma = (2\pi)^{-5} \frac{M_N^2}{8W^2} \frac{q^* p}{\omega_\gamma} \frac{1}{4} \sum_{\text{spins}} |t_\lambda^{\mu_1\mu_2}(\vec{q}_1, \vec{q}_2, \vec{k})|^2 dw_{\pi\pi} d\Omega_{q^*} d\Omega_p, \quad (3)$$

where  $W$  denotes the total c.m. energy,  $\vec{p} = -(\vec{q}_1 + \vec{q}_2)$  the final nucleon momentum, and the variables  $w_{\pi\pi}$  and  $\vec{q}^*$  stand for the invariant  $\pi\pi$  mass and the relative momentum in the c.m. system of the two pions, respectively. The spin structure of the reaction amplitude can be expressed in terms of the nucleon Pauli spin matrices as

$$t_\lambda^{\mu_1\mu_2}(\vec{q}_1, \vec{q}_2, \vec{k}) = K_\lambda^{\mu_1\mu_2}(\vec{q}_1, \vec{q}_2, \vec{k}) + i \vec{L}_\lambda^{\mu_1\mu_2}(\vec{q}_1, \vec{q}_2, \vec{k}) \cdot \vec{\sigma}. \quad (4)$$

Since two pseudoscalar mesons are produced,  $K^{\mu_1\mu_2}$  must be a scalar and  $\vec{L}^{\mu_1\mu_2}$  a pseudovector.

The corresponding isospin decomposition reads, as is discussed in detail in Appendix A (see Eq. (A.10)),

$$t_\lambda^{\mu_1\mu_2}(\vec{q}_1, \vec{q}_2, \vec{k}) = \sum_{l=1}^3 \left( f_l^{(+)}(\vec{q}_1, \vec{q}_2, \vec{k}) \mathcal{O}_{\mu_1\mu_2}^{l(+)} + f_l^{(-)}(\vec{q}_1, \vec{q}_2, \vec{k}) \mathcal{O}_{\mu_1\mu_2}^{l(-)} \right), \quad (5)$$

where the operators  $\mathcal{O}_{\mu_1\mu_2}^{l(\pm)}$  are defined in Eqs. (A.5) through (A.9). The spin-spatial functions  $f_l^{(\pm)}$  depend only on the pion momenta and are independent of their charges  $\mu_1$  and  $\mu_2$ . They have an analogous spin structure as in (4). The functions  $f_l^{(+)}$  are symmetric with respect to the two pion momenta and contribute to two-pion states with total isospin  $T = 0, 2$ , and the  $f_l^{(-)}$  are antisymmetric and contribute to  $T = 1$  states only.

Our calculation of the reaction amplitude  $t^{\mu_1\mu_2}$  follows the same lines as in [2, 3, 4, 10]. Namely, we use the traditional phenomenological Lagrangean approach with Born and resonance contributions on the tree level. Multiple scatterings within the  $\pi N$  and  $\pi\pi$  subsystems are effectively taken into account by introducing nucleon and meson resonances, respectively. For the resonance contributions, the final two-pion state then results from a two-step decay via intermediate quasi-two-body channels for which we take here  $\pi\Delta$ ,  $\rho N$  and  $\sigma N$  channels. Thus the corresponding amplitude can be presented schematically in the form

$$t = t^B + t^{\pi\Delta} + t^{\rho N} + t^{\sigma N}, \quad (6)$$

where  $t^B$  contains all Born terms. The specific diagrams used in the calculation are presented in Fig. 1. Since the operator (6) will be implemented into the deuteron, the corresponding amplitudes are treated non-relativistically with respect to the baryons keeping only terms up to the order  $(p/M_N)$ , denoting the nucleon mass by  $M_N$ .

The resonances included in the model are those which are localized in the mass region up to 1.8 GeV and classified with four stars in the Particle Data Group compilation [11]. Only the  $S_{11}(1650)$  was ignored because of its insignificance. All resonances are listed in Table I. Since we want to consider the reaction up to energies of  $E_\gamma = 1.5$  GeV, resonances with higher spin  $J = 5/2$  and both parities were included. The hadronic coupling constants were fitted to the corresponding decay widths taken from [11]. Their values are listed in Tables II and III. In the quasi-two-body decays  $N^* \rightarrow \pi\Delta$ ,  $N^* \rightarrow \rho N$ , and  $N^* \rightarrow \sigma N$ , the finite widths of  $\Delta$ ,  $\rho$ , and  $\sigma$  were taken into account. As independent parameters, characterizing the electromagnetic transitions  $\gamma N \rightarrow N^*$ , we used the helicity amplitudes also taken from [11]. More details of the formalism are presented in several appendices. The signs of the  $\pi N$  constants are

chosen in such a manner that the multipole amplitudes for pion photoproduction, obtained with our Lagrangeans, are consistent with the corresponding amplitudes of the standard multipole analyses (see e.g. [12]). The choice of the sign for the  $N^* \rightarrow \pi\Delta$  and  $N^* \rightarrow \mu N$  ( $\mu \in \{\rho, \sigma\}$ ) decay amplitudes was based on the  $\pi N \rightarrow \pi\pi N$  analysis of [13].

The next point which deserves a comment is an absorptive effect which is quite well known from photoproduction of vector mesons at high energies. As is discussed in Ref. [14], the absorption follows simply from the existence of many inelastic channels which compete with the process under consideration so that the resulting cross section must essentially be lower than that predicted by the Born approximation alone. Here we follow the prescription of [15] which was used also in [3, 6]. Namely, the  $\Delta$  Kroll-Ruderman term (see diagram (8) of Fig. 1) was multiplied by an energy dependent attenuation factor

$$\eta = \left(1 - Ce^{-(J-1/2)Aq^2/2}\right)^{1/2}, \quad (7)$$

with  $J = 3/2$  as the total  $\pi\Delta$  angular momentum. The  $\pi\Delta$  c.m. momentum is denoted by  $q$ , and the parameter values  $C = 1$  and  $A = 8 \text{ GeV}^{-2}$  were taken from [6]. The same prescription was employed for  $\Delta$  exchange in the  $u$ -channel (second diagram of (14) of Fig. 1) where we assume a weak angular dependence of the  $\Delta$   $u$ -pole propagator, at least at forward angles. For the  $\rho$  Kroll-Ruderman term (diagram (4)) we have taken for the attenuation factor  $C = 1$  and  $A = 5.5 \text{ GeV}^{-2}$  [6]. In this case  $q$  denotes the  $\rho$ -meson c.m. momentum. As one can see from (7) with  $C = 1$ , the  $J = 1/2$  part vanishes completely because of absorption, and the resulting contribution from charged  $\rho$ -photoproduction (Fig. 4) turns out to be relatively small.

For those diagrams containing a meson exchange in the  $t$  channel (diagrams (2), (5)-(7), (9), and (10) of Fig. 1) we adopt the sharp cutoff approximation of [16]. It is based on the assumption that the final particles are completely absorbed within a sphere of radius  $R$ . Then the dependence of the amplitude on the invariant Mandelstam variable  $t$  is changed as follows

$$\begin{aligned} \frac{1}{t - \mu^2} &= - \int_0^\infty b db J_0(b\sqrt{-t}) K_0(b\mu) \\ &\rightarrow - \int_R^\infty b db J_0(b\sqrt{-t}) K_0(b\mu) = \frac{R}{t - \mu^2} [\mu J_0(R\sqrt{-t}) K_1(R\mu) - \sqrt{-t} J_1(R\sqrt{-t}) K_0(R\mu)], \end{aligned} \quad (8)$$

where  $J_n$  and  $K_n$  are cylindrical and hyperbolic Bessel functions [17], and  $\mu$  denotes the mass of the exchanged meson. The integration variable  $b$  in (8) can be interpreted as an impact parameter. The radius  $R$  of the absorbing sphere was chosen such that the characteristic decrease of the experimental cross section for  $\pi^+\pi^-$  photoproduction on a proton above  $E_\gamma = 1 \text{ GeV}$  is reproduced. We have taken  $R = 0.15 \text{ fm}$  for all three exchanged mesons  $\pi$ ,  $\rho$  and  $\sigma$ . Due to this absorptive effect, the central part of the final state wave function vanishes leading to a sharpening of the peripheral peak in the angular distribution as is demonstrated in Fig. 2.

As already stressed in the introduction, the quasi-classical nature of this method makes its application doubtful in the second resonance region, where the  $\pi\Delta$  and  $\rho N$  interactions are not of diffractive character, and other aspects of the final state interaction should come into play. Thus we consider this method only as a simple, heuristic possibility to reduce a too strong increase of the cross section above  $E_\gamma = 750 \text{ MeV}$ , which on the other hand can be physically motivated, in contrast to fitting the data with extremely soft form factors.

Our results for the total cross section of two-pion production on the proton are presented in Figs. 3 through 5. The pion photoelectric term (diagram (9) of Fig. 1) is well known to give most of the forward charged  $\pi$  production in the  $\pi\Delta$  channel. The  $\Delta$  Kroll-Ruderman term, needed for restoring gauge invariance of the amplitude, provides an essential part of the total cross section for  $\pi^+\pi^-$  production. With respect to other Born diagrams, as is shown in the lower panel of Fig. 3, important contributions come also from the nucleon Kroll-Ruderman and pion-pole terms (diagrams (1) and (2) of Fig. 1) as well as from the  $N\Delta$  and  $\Delta\Delta$   $s$ - and  $u$ -channels (diagrams (12) and (14) of Fig. 1). Also  $\sigma$  exchange in  $\rho$ -photoproduction (diagram (6)) is responsible for quite a large fraction of the  $\pi^+\pi^-$  cross section above  $E_\gamma = 1.2 \text{ GeV}$ . The remaining Born terms are less important, but their combined effect becomes still significant with increasing energy (long dash-dotted curve in the lower panel of Fig. 3).

In order to compare our results with those of other authors, we present in Figs. 3 through 5 separately the contributions of the individual resonances to the total cross section. The comparison to previous work shows that our model is quite close to that of the Valencia group [2] but differs visibly from the Saclay model [3] which, however, is primarily concerned with the role of the Roper resonance. The only essential difference to [2] lies in the treatment of the  $D_{13}(1520)$  resonance. The spin structure of the  $D_{13} \rightarrow \pi\Delta$  transition used in [2] leads to an additional strong momentum dependence in the  $s$ -wave part of the amplitude, whereas in our case the  $s$ -wave of the  $D_{13} \rightarrow \pi\Delta$  vertex

(see Table IV) remains constant. We will return to this question when the low-energy behavior of the total cross section will be discussed.

For a qualitative analysis of the resonance contributions we write the corresponding total cross section in a simplified form

$$\sigma \approx \frac{\pi}{4\omega_\gamma^2} \sum_{N^*} (2J+1) \Gamma_{\gamma N^*}(W) |G_{N^*}(W)|^2 \Gamma_{N^* \rightarrow \pi\pi N}(W), \quad (9)$$

where the total two-pion decay width  $\Gamma_{N^* \rightarrow \pi\pi N}$  is written as an incoherent sum of the contributions of the various intermediate quasi-two-body channels, i.e.

$$\Gamma_{N^* \rightarrow \pi\pi N} = \Gamma_{N^* \rightarrow \pi\pi N}^{(\pi\Delta)} + \Gamma_{N^* \rightarrow \pi\pi N}^{(\rho N)} + \Gamma_{N^* \rightarrow \pi\pi N}^{(\sigma N)}, \quad (10)$$

which is correct provided one can neglect the overlap between the different resonance amplitudes in (6). One can expect a relatively small interference at least between  $t^{\pi\Delta}$  and  $t^{\rho N}$  because of a relatively small width of the  $\Delta$  and  $\rho$  resonances compared to the mass splitting between the different channels (in the limit of vanishingly small widths the final quasi-two-body states should be orthogonal). Therefore, although for an exact partial wave analysis the overlap between quasi-two-body channels in the observables should be taken into account, this interference is omitted for the moment being. Using Eq. (9), the contribution of an individual resonance  $N^*(J, L)$  at  $W = M_{N^*}$  is estimated as

$$\sigma^{N^*} \approx (2J+1) \frac{\pi}{\omega_\gamma^2} \frac{\Gamma_{\gamma N^*} \Gamma_{N^* \rightarrow \pi\pi N}}{\Gamma_{tot}^2}. \quad (11)$$

It may be instructive to supplement Eq. (11) by the separate contributions of the intermediate quasi-two-body states to the various charge channels of two pion production. Factoring out and evaluating explicitly the isospin matrix elements, one obtains for  $T = \frac{3}{2}$  resonances

$$\begin{aligned} \sigma^{N^*}(\pi^+\pi^-) &= \frac{26}{45} \sigma_{\pi\Delta}^{N^*} + \frac{2}{3} \sigma_{\rho N}^{N^*}, \\ \sigma^{N^*}(\pi^+\pi^0) &= \frac{17}{45} \sigma_{\pi\Delta}^{N^*} + \frac{1}{3} \sigma_{\rho N}^{N^*} = \sigma^{N^*}(\pi^-\pi^0), \\ \sigma^{N^*}(\pi^0\pi^0) &= \frac{2}{45} \sigma_{\pi\Delta}^{N^*}, \end{aligned} \quad (12)$$

and for  $T = \frac{1}{2}$  resonances

$$\begin{aligned} \sigma^{N^*}(\pi^+\pi^-) &= \frac{5}{9} \sigma_{\pi\Delta}^{N^*} + \frac{1}{3} \sigma_{\rho N}^{N^*} + \frac{2}{3} \sigma_{\sigma N}^{N^*}, \\ \sigma^{N^*}(\pi^+\pi^0) &= \frac{2}{9} \sigma_{\pi\Delta}^{N^*} + \frac{2}{3} \sigma_{\rho N}^{N^*} = \sigma^{N^*}(\pi^-\pi^0), \\ \sigma^{N^*}(\pi^0\pi^0) &= \frac{2}{9} \sigma_{\pi\Delta}^{N^*} + \frac{1}{3} \sigma_{\sigma N}^{N^*}. \end{aligned} \quad (13)$$

Here the partial cross sections  $\sigma_X^{N^*}$  ( $X \in \{\pi\Delta, \rho N, \sigma N\}$ ) are obtained from Eq. (11) by substituting the total  $\pi\pi N$  width  $\Gamma_{N^* \rightarrow \pi\pi N}$  by the partial width  $\Gamma_{N^* \rightarrow \pi\pi N}^{(X)}$ . As discussed above, these relations are exact only for vanishing overlap between the quasi-two-body channels, and in practice should be used for qualitative estimates only. On the other hand, a comparison of the straightforward evaluation shows that the approximations (11) through (13) reproduce indeed quite well the actual resonance contribution to the total cross section. Only for those resonances, which are strongly coupled to  $\sigma N$  channel the cross section is sensitive to the sign of the  $N^* \rightarrow \sigma N$  coupling, primarily because of a large width of the  $\sigma$  meson. Evaluating (13) for the Roper resonance  $P_{11}(1440)$ , one finds a contribution of about  $0.8 \mu\text{b}$  to the  $\pi^0\pi^0$  cross section at  $E_\gamma = 635 \text{ MeV}$ , which totally excludes its dominance in this channel. This result is consistent with the calculation of [2] and is at variance with the theoretical prediction of [23]. The role of the  $S_{11}(1535)$  resonance, which is often ignored in  $\pi\pi$  photoproduction models, is almost as important as that of  $P_{11}(1440)$ . Furthermore, comparing (12) with (13) for the  $\pi^0\pi^0$  channel, one readily sees that the contribution of  $T = 3/2$  resonances to this channel should be small in general.

As is shown in Figs. 3 through 5, the  $D_{13}(1520)$  provides the dominant resonance contribution to double pion photoproduction in the second resonance region. A significant role of the  $D_{33}(1700)$  and  $F_{15}(1680)$  is also worth noting. Other resonances are less pronounced. We would like to stress the fact that we did not fit the resonance parameters to the observed cross sections. Therefore, the quality of the description of the data in Fig. 3 through 5

is not perfect. In particular we do not reproduce the position of the second peak observed in the  $\pi^+\pi^-$  and  $\pi^0\pi^0$  channels. Also the  $\pi^+\pi^0$  experimental cross section is underestimated in the region below  $E_\gamma = 0.7$  GeV.

In addition, there is no room in our model for a large contribution of the  $D_{33}(1700)$  resonance. As was already noted in [24], having a large width and a strong coupling to the  $s$ -wave  $\pi\Delta$  state, this resonance can interfere with the  $\Delta$  Kroll-Ruderman term and, therefore, influences the resulting cross section over a wide energy region. One should notice that analogously to  $D_{13}(1520)$ , the  $D_{33}(1700)$  resonance tends to increase the total cross section for  $\pi^+\pi^-$  production, in contrast to the results of [24], where its inclusion reduces the  $\pi^+\pi^-$  cross section. The analysis of [13] gives opposite signs for the decay amplitudes  $D_{13}(1520) \rightarrow \pi\Delta$  and  $D_{33}(1770) \rightarrow \pi\Delta$  with respect to the corresponding  $\pi N$  decay amplitudes. But from the multipole analysis of pion photoproduction follows that the  $\pi N$  vertices of these resonances have also opposite signs (see Table IV), so that the total phase of both amplitudes is the same. As one can see in Fig. 3, including  $D_{33}(1700)$ , one obtains a sizeable overestimation of the data. We cannot, however, conclude that our evaluation tends to favor a less important role of this resonance in double pion photoproduction than the one using the parameters given in [11]. More likely, this inconsistency points to shortcomings in the Born amplitude, whose role may well be overestimated by the present model.

For  $\pi^0\pi^0$  photoproduction, our calculation predicts a second peak at  $E_\gamma = 1$  GeV mostly coming from the excitation of the  $F_{15}(1680)$  resonance. Its position is in rough agreement with experiment [23], but its magnitude is considerably underestimated. However, one can obtain a much better description of the experimental cross section in this region (dotted curve in Fig. 5) by choosing instead of a negative sign of the  $F_{15}\pi\Delta$  coupling from [13] a positive one as predicted in [1]. In Ref. [23], the second peak in the  $\pi^0\pi^0$  data was explained as an interference effect between the  $P_{11} \rightarrow \sigma N \rightarrow \pi^0\pi^0 N$  mechanism and a very strong background from photoproduction of a  $\sigma$  meson via  $\rho$  exchange (diagram (7) of Fig. 1). However, in the present model, the background from intermediate  $\sigma$  photoproduction, for which our model predicts about  $0.5 \mu\text{b}$  at  $E_\gamma = 1$  GeV, turns out to be rather insignificant. We did not include in the calculation the  $P_{11}(1710)$  resonance, but a simple estimate, using the expressions of (11) and (13), gives for the  $P_{11}(1710) \rightarrow \sigma N \rightarrow \pi^0\pi^0 N$  mechanism only about  $0.3 \mu\text{b}$  at the same energy, so that the combined contribution from these terms does not strongly influence the  $\pi^0\pi^0$  cross section.

In Fig. 6 we show the cross section for  $\rho$ -meson photoproduction. In this case we have extended the calculation up to  $E_\gamma = 3$  GeV in order to show the trend of the cross section at higher energies. In  $\rho^0$  meson production, the charge conjugation invariance forbids the exchange of vector mesons, so that only spin-zero mesons can contribute to  $t$ -channel exchange. As is shown in Fig. 6, within the present model, most of neutral  $\rho$  production comes from  $\sigma$ -exchange (diagram (6) in Fig. 1), except for the “subthreshold” region, i.e.  $E_\gamma < 1$  GeV, which is dominated by baryon resonance excitations. The role of  $\pi$ -exchange remains insignificant, primarily, because of a very weak coupling at the  $\gamma\pi^0\rho^0$  vertex. Although the dominance of the  $\gamma(\pi\pi)$  mode in the radiative  $\rho^0$ -meson decay can serve as a strong justification for the  $\sigma$ -exchange model, its status in the theory of  $\rho^0$  production is not clear. There are more refined models (see e.g. [26] and references therein) which are however much more complicated.

Without the  $D_{33}(1700)$  resonance, one obtains a satisfactory agreement with the cross section data for  $\pi^+\pi^-$  and  $\pi^+\pi^0$  production, but there is a sizeable deviation for the  $\pi^0\pi^0$  channel. In the region up to  $E_\gamma < 0.7$  GeV, the theoretical results lie far below the experimental points so that the data can not be fitted simply by varying the parameters of resonances. The relatively steep rise of the experimental cross section in Fig. 5 right above the threshold indicates quite a strong  $s$ -wave contribution to the production amplitude, which, however, is not born out by our model. But in order to reach a more definite conclusion with respect to the partial wave structure of the amplitude, one needs experimental angular distributions of the produced particles. Of the various Born amplitudes, which contribute to the  $s$ -wave part, only the  $N\Delta$  crossed term (the second diagram of (12) of Fig. 1) appears to be relatively important at low energies (dash-dotted curve in the left panel of Fig. 5), but its contribution is, however, not sufficient to explain the observed cross section. Also the so-called  $Z$ -graphs do not seem to play a sizeable role. As an example, we demonstrate in Fig. 5 the importance of the diagram (17) where the final  $\pi^0\Delta^+$  state can be produced in an  $s$ -wave via photoabsorption on an antinucleon. It is the only possibility to leave the  $\pi\Delta$  system in a relative  $s$ -state. Other possible couplings with an antinucleon lead to higher partial  $\pi\Delta$  waves and should be much less important near threshold. As one can see from Fig. 5, the  $Z$ -graph plays only a secondary role and cannot explain the rapid rise of the experimental cross section just above threshold.

With respect to the resonance mechanisms, our calculation predicts a relatively small contribution from  $D_{13}(1520)$  around a photon energy of  $E_\gamma = 0.6$  GeV, which is about three times smaller than the one in Ref. [2]. The possible reason for this difference was already partially explained above. Namely, the negative  $q^2$ -dependent contribution to the  $s$ -wave amplitude in [2] requires on the other hand a much stronger momentum independent part at low energy than in our model, thus making the energy dependence of the cross section less pronounced. Here we do not discuss such effects like  $\pi^+\pi^- \rightarrow \pi^0\pi^0$  scattering, considered in [29] at very low energies, as well as the influence of the type of  $\pi NN$  coupling, discussed in [30]. In any case, because of such a strong model dependence of the low energy  $\pi^0\pi^0$  cross section, more refined theoretical and experimental investigations of this channel are needed. In general, it should be noted, that there is no qualitative agreement between different authors with respect to the contribution of the

$D_{13}(1520)$  resonance. Even at the resonance peak around  $E_\gamma = 0.75$  GeV, where the value of the cross section is fixed almost unambiguously by the electromagnetic and hadronic decay widths (see Eq. (11)), the size of the cross section varies very strongly. For example, in the  $\pi^+\pi^0$  channel, the contribution of the  $D_{13}(1520)$  is about  $30 \mu\text{b}$  in [4] but only  $20 \mu\text{b}$  in [2] and in our work.

As for the reaction on the neutron, one notes in Fig. 7 that the  $\pi^+\pi^-n$  and  $\pi^-\pi^0n$  cross sections are practically equal to the corresponding  $\pi^+\pi^-p$  and  $\pi^+\pi^0p$  cross sections. Comparison with the old data for  $\pi^+\pi^-n$  [31] shows that the theory gives values systematically higher than the experimental results by about 20 % at the maximum of the cross section.

In Fig. 8 we present our results for the beam-target helicity asymmetry of the total cross section

$$\Delta\sigma = \sigma_{3/2} - \sigma_{1/2}, \quad (14)$$

where  $\sigma_\lambda$  corresponds to the total cross section for parallel orientation of photon and target spins for  $\lambda = 3/2$  and to the antiparallel orientation for  $\lambda = 1/2$ . In comparison to our previous calculation [27], inclusion of higher resonances as well as a more refined treatment of the Born terms shifts  $\Delta\sigma$  above the  $D_{13}(1529)$  peak to negative values, especially in the  $\pi^+\pi^-$  and  $\pi^0\pi^0$  channels. Again, in the low energy region we find a significant deviation of our results for  $\pi^0\pi^0$  production from the preliminary data of [28]. In order to analyze the present results, we write the resonance contribution to the asymmetry (14) in the simplified form

$$\Delta\sigma \approx \frac{\pi}{2\omega_\gamma^2} \sum_{N^*} (2J+1) \{ \Gamma_{\gamma N^*}^{3/2}(W) - \Gamma_{\gamma N^*}^{1/2}(W) \} |G_{N^*}(W)|^2 \Gamma_{N^* \rightarrow \pi\pi N}(W), \quad (15)$$

which is obtained under the same assumptions as (9). The partial widths  $\Gamma_{\gamma N^*}^j(W)$  ( $j = 1/2, 3/2$ ) are defined in Appendix B in (B.12). The  $D_{13}(1520)$  resonance, for which one finds  $\Gamma_{\gamma N^*}^{3/2} \approx 14 \Gamma_{\gamma N^*}^{1/2}$  [11] at  $W = M_{D_{13}}$  on the proton, contributes thus almost exclusively to the  $3/2$  part. However, as one can see from Fig. 8, the positive contribution of  $D_{13}$  to  $\Delta\sigma$  is more than canceled by a negative contribution of the  $P_{11}$  resonance at low energies. Furthermore, the Born terms alone exhibit a very small helicity dependence resulting in a strong cancellation between  $\sigma_{3/2}$  and  $\sigma_{1/2}$  (dashed curve in the lower right panel of Fig. 8). As a result, we obtain an essentially negative value for the asymmetry (14) around  $E_\gamma = 0.6$  GeV. This is in disagreement with the experimental results obtained at MAMI [28] as well as with the calculation of [30] where this asymmetry amounts at this energy up to about  $+5 \mu\text{b}$ . Probably, the crucial origin of this disagreement lies in the mentioned strong model dependence of the Born sector.

Finally, Fig. 9 shows the result of our calculation of the beam asymmetry  $\Sigma$  for linearly polarized photons in the  $\pi^0\pi^0$  photoproduction, which is compared to the recent GRAAL data [23]. Although in the first energy bin one notes satisfactory agreement, one clearly sees for the higher energies an increased deviation from the experimental results which exhibit a slightly negative asymmetry in contrast to a positive asymmetry of the theory.

### III. DOUBLE PION PHOTOPRODUCTION ON THE DEUTERON

We will now turn to incoherent two-pion photoproduction on the deuteron

$$\gamma(k, \vec{\epsilon}_\lambda) + d(p_d) \rightarrow \pi^{\mu_1}(q_1) + \pi^{\mu_2}(q_2) + N_1(p_1) + N_2(p_2), \quad (16)$$

The corresponding coherent process (without deuteron break up) in the "neutral" channels  $\pi^+\pi^-$  and  $\pi^0\pi^0$  has a very small cross section and will be considered very briefly at the end of the section.

The reaction (16) is in principle considerably more complex than the reaction on the nucleon, because in addition to the production on each of the two nucleons one would have to consider electromagnetic two-body production operators. The latter, however, will be neglected in the present work. Thus the e.m. interaction consists in the sum of the one-body production operators, which often is called the impulse approximation (IA) if in addition the interaction between the various particles in the final state (FSI) is neglected. But in the present work, we will at least include the interaction between the two final nucleons.

In the  $\gamma d$  c.m. system, the spin-averaged cross section of the reaction (16) then reads

$$d\sigma = (2\pi)^{-8} \frac{E_d M_N^2 Q p^* q^*}{8W^2 \omega_\gamma} \frac{1}{6} \sum_{\lambda, M_d} \sum_{S, M_S} \left| \sum_{I=0,1} T_{IM_I S M_S \lambda M_d}^{\mu_1 \mu_2}(\vec{q}_1, \vec{q}_2, \vec{p}, \vec{k}) \right|^2 d\Omega_Q d\omega_{NN} d\omega_{\pi\pi} d\Omega_{p^*} d\Omega_{q^*}, \quad (17)$$

where  $\vec{Q} = \vec{q}_1 + \vec{q}_2$  denotes the total 3-momentum of the two final pions,  $\omega_{\pi\pi}$  the invariant  $\pi\pi$  mass,  $\vec{q}^*$  the relative momentum in the  $\pi\pi$  restsystem, and  $\omega_{NN}$  and  $\vec{p}^*$  the corresponding quantities for the  $NN$  subsystem, whereas  $\vec{p}$

denotes the relative two-nucleon momentum in the overall  $\gamma d$  c.m. system. Furthermore,  $T$  stands for the reaction matrix, in which the e.m. interaction is represented by the sum of the two-pion production amplitudes on each of the nucleons, i.e.

$$T_{IM_I SM_S \lambda M_d}^{\mu_1 \mu_2}(\vec{q}_1, \vec{q}_2, \vec{p}, \vec{k}) = {}^{(-)}\langle \vec{p}; SM_S; IM_I | \left( \hat{t}_\lambda^{\mu_1 \mu_2, (1)}(\vec{q}_1, \vec{q}_2, \vec{k}) + \hat{t}_\lambda^{\mu_1 \mu_2, (2)}(\vec{q}_1, \vec{q}_2, \vec{k}) \right) | 1M_d; 00 \rangle, \quad (18)$$

where  $t_\lambda^{\mu_1 \mu_2, (i)}$  denotes the elementary production operator on nucleon “ $i$ ”.

The final two-nucleon state, characterized by the total spin  $S$  and isospin  $I$  and the corresponding projections  $M_S$  and  $M_I$ , is represented by a relative scattering wave  $|\vec{p}; SM_S; IM_I\rangle^{(-)}$  which is determined by the  $NN$  scattering matrix  $t_{NN}$

$$|\vec{p}; SM_S; IM_I\rangle^{(-)} = \left( 1 + t_{NN} G_{NN}(W_{NN} - i\epsilon) \right) \frac{1}{\sqrt{2}} \left[ |\vec{p}\rangle - (-1)^{S+I} |-\vec{p}\rangle \right] |SM_S\rangle |IM_I\rangle, \quad (19)$$

where  $|\vec{p}\rangle$  denotes a relative two-nucleon plane wave and  $G_{NN}$  the free relative  $NN$  propagator.

According to the two contributions to the final  $NN$  state in (19) the reaction matrix  $T$  may be split into two terms, the standard impulse approximation (IA) or spectator model as the basic part and the rescattering contribution of the nucleons in the final state, so that the resulting amplitude is given by

$$T_{IM_I SM_S \lambda M_d}^{\mu_1 \mu_2}(\vec{q}_1, \vec{q}_2, \vec{p}, \vec{k}) = T_{IM_I SM_S \lambda M_d}^{\mu_1 \mu_2, (IA)}(\vec{q}_1, \vec{q}_2, \vec{p}, \vec{k}) + T_{IM_I SM_S \lambda M_d}^{\mu_1 \mu_2, (NN)}(\vec{q}_1, \vec{q}_2, \vec{p}, \vec{k}). \quad (20)$$

Denoting the matrix element of the elementary production on a nucleon with initial momentum  $\vec{p}_i$  by  $t_\lambda^{\mu_1 \mu_2}(\vec{q}_1, \vec{q}_2, \vec{p}_i, \vec{k})$ , the amplitude of the IA-term reads

$$\begin{aligned} T_{IM_I SM_S \lambda M_d}^{\mu_1 \mu_2, (IA)}(\vec{q}_1, \vec{q}_2, \vec{p}, \vec{k}) &= \sqrt{2} \sum_{M'_S} \langle IM_I | \langle SM_S | \left[ t_\lambda^{\mu_1 \mu_2}(\vec{q}_1, \vec{q}_2, \frac{1}{2}\vec{Q} + \vec{p} - \vec{k}, \vec{k}) \Psi_{M'_S M_d} \left( \frac{1}{2}(\vec{Q} - \vec{k}) + \vec{p} \right) \right. \\ &\quad \left. - (-1)^{S+I} t_\lambda^{\mu_1 \mu_2}(\vec{q}_1, \vec{q}_2, \frac{1}{2}\vec{Q} - \vec{p} - \vec{k}, \vec{k}) \Psi_{M'_S M_d} \left( \frac{1}{2}(\vec{Q} - \vec{k}) - \vec{p} \right) \right] | 1M'_S \rangle | 00 \rangle, \end{aligned} \quad (21)$$

where  $\Psi_{M_S M_d}$  represents the component of the deuteron wave function with a definite two-nucleon spin projection  $M_S$

$$\Psi_{M_S M_d}(\vec{p}) = \sum_{L=0,2} (LM_L 1M_S | 1M_d) u_L(p) Y_{LM_L}(\hat{p}). \quad (22)$$

The rescattering term in (20) is given by

$$T_{IM_I SM_S \lambda M_d}^{\mu_1 \mu_2, (NN)}(\vec{q}_1, \vec{q}_2, \vec{p}, \vec{k}) = \sum_{M'_S} \int \frac{d^3 p'}{(2\pi)^3} t_{IM_I S, M'_S M_S}^{NN}(\vec{p}, \vec{p}') G_{NN}(W_{NN}) T_{IM_I SM_S \lambda M_d}^{\mu_1 \mu_2, (IA)}(\vec{q}_1, \vec{q}_2, \vec{p}', \vec{k}), \quad (23)$$

where  $t^{NN}$  denotes the half off-shell  $NN$  scattering matrix. In the calculation of the integral in (23) we use a partial wave decomposition of the  $NN$  scattering states.

The isospin structure of the amplitude is easily evaluated using (5) with the isospin operators listed in (A.5) through (A.9)

$$\langle 00 | t^{\mu_1 \mu_2} | 00 \rangle = \delta_{\mu_1, -\mu_2} \left( (-1)^{\mu_1} f_1^{(+)} + \mu_1 f_2^{(-)} \right), \quad (24)$$

$$\begin{aligned} \langle 1M_I | t^{\mu_1 \mu_2} | 00 \rangle &= \delta_{M_I, 0} \delta_{\mu_1, -\mu_2} \left( (-1)^{\mu_1} f_2^{(+)} - \mu_1 f_1^{(-)} \right) + \frac{1}{2} \left( (-1)^{\mu_2} \delta_{\mu_1, 0} \delta_{M_I, -\mu_2} + (\mu_1 \leftrightarrow \mu_2) \right) f_3^{(+)} \\ &\quad - \left( \mu_1 \delta_{\mu_2, 0} \delta_{M_I, -\mu_1} - (\mu_1 \leftrightarrow \mu_2) \right) f_1^{(-)} - \frac{1}{2} \left( (-1)^{\mu_2} \delta_{\mu_1, 0} \delta_{M_I, -\mu_2} - (\mu_1 \leftrightarrow \mu_2) \right) f_3^{(-)}. \end{aligned} \quad (25)$$

Since calculational details associated with the evaluation of the two-nucleon interaction in incoherent meson production on the deuteron were considered in many papers (see, e.g. [32, 33, 34]) there is no need to repeat them here. We only note that  $S$ ,  $P$ , and  $D$  waves were included in the  $NN$  scattering matrix, for which the separable version of the Paris potential from [35] was used. For the sake of consistency, also the deuteron wave function was calculated using the separable form of the potential.

As our main result, we present in Fig. 10 the total cross sections for the various charge configurations of  $\pi\pi$  photoproduction on the deuteron. The cross sections reproduce qualitatively the form of the elementary cross section

(dotted curves) except that they are slightly smeared out by the Fermi motion especially around the resonance peaks. This fact together with the obviously quite small influence of  $NN$  rescattering in the final state support the approximate validity of the spectator model. Even in the "neutral"  $\pi^+\pi^-$  channel, which is by far the most important channel, FSI leads to a lowering by only 10 % of the plane wave cross section. Thus it is significantly smaller than what had been found in single neutral pion production on the deuteron  $\gamma d \rightarrow \pi^0 np$  where this effect lead to a reduction by about 30 %.

This feature is easily explained by the relatively large momentum transfer associated with the production of two pions. Firstly, it leads to a reduction of the region of small distances between the nucleons, where the  $NN$  interaction is sizeable. Furthermore, more importantly in the neutral channel where also the coherent transition (without deuteron break up) is possible, is the nonorthogonality of the initial and final  $NN$  wave functions in IA. As a consequence, the IA contains part of the coherent reaction. The size of this "nonorthogonal contribution" is roughly given by the coherent cross section (see e.g. [36]) and depends strongly on the momentum transfer to the  $NN$  subsystem (in the extreme case when the momentum transfer goes to zero, the IA contains it completely). In particular, this effect leads to a large role of  $NN$  FSI in the single  $\pi^0$  photoproduction on the deuteron where the coherent channel turns out to be quite sizeable. Again, the role of orthogonality in the  $\pi\pi$  reactions is reduced because of a significantly increased momentum transfer. Comparison with the available data in Fig. 10 shows that the agreement in the  $\pi^+\pi^-$  and  $\pi^-\pi^0$  channels is quite satisfactory. Deviation from the  $\pi^0\pi^0$  data should arise from the same origin as that discussed above for the corresponding elementary reaction.

The coherent cross sections in the  $\pi^+\pi^-$  and  $\pi^0\pi^0$  channels are presented in Fig. 11. In contrast to the single pion case, the coherent  $\pi^+\pi^-$  photoproduction comprise only about 6 % of the corresponding incoherent cross sections in Fig. 10. The  $\gamma d \rightarrow \pi^0\pi^0 d$  cross section turns out to be vanishingly small. In the last case only the symmetric part, proportional to  $f_1^{(+)}$  in (24) contributes. For the resonances with isospin  $T=1/2$  it is determined by the isoscalar part of the  $\gamma N \rightarrow N^*$  transition (see Table V), which is small for almost all resonances considered here. For  $T=3/2$  resonances as well as for most of the Born terms, which are important in the elementary  $\pi^0\pi^0$  photoproduction, the amplitude  $f_1^{(+)}$  is zero (see Table V). As a result, the coherent  $\pi^0\pi^0$  cross section comprises about 0.5 % of the incoherent one.

Finally, we present in Fig. 12 the beam-target helicity asymmetry  $\Delta\sigma$ , defined analogously as the one for the elementary reaction on a nucleon (14),

$$\Delta\sigma = \sigma^P - \sigma^A, \quad (26)$$

where  $\sigma^{P/A}$  correspond to the total cross section for parallel/antiparallel orientation of photon and target spins, respectively. As in the elementary case, these asymmetries exhibit positive maxima around 700-750 MeV corresponding to the contribution of the  $D_{13}(1520)$  resonance and then decrease rapidly with increasing energy towards negative values above roughly 1.2 GeV. Compared to our earlier evaluation [27], this feature reduces substantially the two-pion contribution to the Gerasimov-Drell-Hearn (GDH) integral. The results of the explicit integration up to 1.5 GeV are listed in Table VI together with the finite total GDH-integral including  $\pi$ ,  $\eta$ , and  $\pi\pi$  contributions, and photodisintegration in case of the deuteron. For the neutron one notices a substantial underestimation of the GDH value by about 40  $\mu\text{b}$ , while for the proton only a slight overestimation is found. For the deuteron a positive contribution of about 29  $\mu\text{b}$  is missing.

Concluding this section we would like to comment on some restrictions of our results. As is stressed above, the corrections from the  $NN$  interaction are relatively small. However, the conclusion about the general validity of the spectator model for the photoproduction on the deuteron has to be confronted with the experimental results of [39]. In this paper the transition  $\gamma d \rightarrow \Delta^{++}\Delta^-$  with subsequent decay to the  $pn\pi^+\pi^-$  state was extracted, using the analysis of the  $\pi N$  invariant mass distributions. The crucial point is that for this transition to happen both nucleons have to participate actively in the reaction, quite in contrast to the present treatment, where the second nucleon takes part only in the distortion of the final  $NN$  waves. According to the measured yields, the two-body mechanism provides about 30 % of the total cross section, thus making the validity of the spectator model very doubtful. This conclusion was confirmed by the calculation presented in [40] where the transition to the  $\Delta^{++}\Delta^-$  state amounts to 40  $\mu\text{b}$  at  $E_\gamma = 800$  MeV. Assuming a two-step mechanism one could naively estimate that it would lead to a contribution comparable in size with pion rescattering in single pion photoproduction on the deuteron. However, this last effect was shown to be vanishingly small [32, 33]. Thus we think, this aspect deserves a more detailed study.

#### IV. SUMMARY AND CONCLUSIONS

In the present paper, we have extended the elementary two-pion photoproduction operator used in previous work [2, 3, 4] to higher energies, including all four-star resonances with masses  $M < 1.8$  GeV. This operator is based on an



effective Lagrangean approach evaluating only tree-level diagrams. The necessary coupling strengths are determined by the hadronic and electromagnetic decays of the resonances. The present approach does not allow a high precision description of the reaction, primarily because of a nonrelativistic treatment of the baryons and other shortcomings. However, it should be able to account for the main features of the reaction so that at least qualitative conclusions about the underlying mechanisms can be drawn.

In the  $\pi^+\pi^-$  and  $\pi^+\pi^0$  channels it is quite easy to obtain a decent description of the data, but only if the large contribution of  $D_{33}(1700)$  is excluded. Furthermore, we face principal difficulties in the  $\pi^0\pi^0$  channel, where the theory strongly underestimates the cross section data in the near threshold region below  $E_\gamma=0.7$  GeV. It should be stressed that from all charge channels the  $\pi^0\pi^0$  one is the least understood, but it is also the weakest one, less than 15 % of the dominant  $\pi^+\pi^-$  channel. Apart from the noted underestimation at low energies, there is also a visible deviation between experimental and theoretical results for the  $\Sigma$  asymmetry for linearly polarized photons as well as for the  $\pi^0\pi^0$  photoproduction on a neutron as was noted in [23] and [8]. We think that more detailed studies of angular distributions as well as polarization measurements can help to clarify the role of different mechanisms in the  $\pi\pi$  photoproduction in the second resonance region. In particular, the investigation of the beam asymmetry with the CLASS detector [41] seems to be very promising for studying the structure of the production amplitude.

A major unresolved problem is the role of final state interaction in the  $\pi\pi N$  system which is also closely connected to the problem of unitarity and analyticity of the overall production amplitude. In the present paper we took into account only quite roughly the effect of absorption in the final state within the WKB prescription. Although this quasi-classical method is used also at low energies, its validity should be doubted in the second resonance region, where only the lowest partial waves dominate the cross section. As an alternative approach, the method used in [5] treats the  $\pi NN$  interaction as an effective quasi-two-body scattering via resonance excitations. But we think, it is not clear whether such a simplified approach to the  $\pi\pi N$  system can account for its quite complicated dynamics. For a more realistic treatment of the  $\pi\pi N$  interaction, a rigorous three-body scattering approach is needed, where not only two-body but also three-body unitarity of the  $\pi\pi N$  interaction can be systematically incorporated. Because of quite a large amount of resonances involved in  $\pi N$  scattering, a full analysis of the  $\pi\pi N$  system appears to be quite complex. However, a first and apparently very good approximation is provided by taking into account only the  $\Delta(1232)$  resonance in the  $\pi N$  and the  $\sigma$ -resonance in the  $\pi\pi$  subsystem.

As for the reaction on the deuteron, our primary aim was to investigate the role of the  $NN$  interaction between the final nucleons, thus testing the validity of the spectator model. The main result is that the effect of the  $NN$  interaction is quite small. From this point of view, the spectator model can be considered as a good first approximation for a rough determination of the elementary neutron amplitude from the deuteron data in the region of quasifree kinematics. However, for precision studies, although at present out of sight, such FSI and other nuclear effects have to be considered with care.

Concluding the paper, we would like to mention, that in our opinion, future work should be oriented not only to a refinement of the  $\pi\pi$ -photoproduction model, but more importantly to a unification of the models for single and double pion photoproduction. In other words, a consistent treatment providing at the same time an at least reasonable description for both channels would be more useful, than an excellent but independent fit of these two types of reactions, achieved with very different sets of parameter values.

## APPENDIX A: THE ISOTOPIC SPIN STRUCTURE OF THE $\gamma N \rightarrow \pi\pi N$ AMPLITUDE

In this appendix we discuss the isotopic spin structure of the amplitude for double pion photoproduction. Our goal is to present the production amplitude as an operator in the nucleon isotopic spin space, analogously to what is done for single pion photoproduction [42], where the existence of three independent charge channels is described by three corresponding isospin operators

$$t(\gamma N \rightarrow \pi^\mu N) = A^{(0)}\tau_\mu^\dagger + A^{(-)}\frac{1}{2}[\tau_\mu^\dagger, \tau_0] + A^{(+)}\frac{1}{2}\{\tau_\mu^\dagger, \tau_0\}. \quad (\text{A.1})$$

Our convention for the isospin operators are

$$\tau_0 = \tau_z \quad \text{and} \quad \tau_{\pm 1} = \mp \frac{1}{\sqrt{2}}(\tau_x \pm i\tau_y), \quad (\text{A.2})$$

where  $\vec{\tau}$  denotes the Pauli isospin operator, so that

$$\langle p|\tau_1|n\rangle = -\langle n|\tau_{-1}|p\rangle = -\sqrt{2}, \quad \langle p|\tau_0|p\rangle = -\langle n|\tau_0|n\rangle = 1. \quad (\text{A.3})$$

In double pion production one has six independent charge channels, which are described by six isospin operators  $\mathcal{O}_{\mu_1\mu_2}$ , depending on  $\tau_{\mu_1}^\dagger$  and  $\tau_{\mu_2}^\dagger$ . Since the amplitude  $t^{\mu_1\mu_2}$  has to be symmetric under interchange of the two pions because of their boson property, i.e.

$$t^{\mu_1\mu_2}(\vec{q}_1, \vec{q}_2, \vec{k}) = t^{\mu_2\mu_1}(\vec{q}_2, \vec{q}_1, \vec{k}), \quad (\text{A.4})$$

the operators  $\mathcal{O}_{\mu_1\mu_2}$  can be chosen with definite symmetry property. It turns out that three of them are symmetric under interchange  $\mu_1 \leftrightarrow \mu_2$ , denoted by a superscript “(+)”, and the other three antisymmetric with superscript “(-)”

$$\mathcal{O}_{\mu_1\mu_2}^{1(+)} = \frac{1}{2}\{\tau_{\mu_2}^\dagger, \tau_{\mu_1}^\dagger\} = (-1)^{\mu_1}\delta_{\mu_1, -\mu_2}, \quad (\text{A.5})$$

$$\mathcal{O}_{\mu_1\mu_2}^{1(-)} = \frac{1}{2}[\tau_{\mu_2}^\dagger, \tau_{\mu_1}^\dagger] = \sqrt{2}(1\mu_1 1\mu_2 | 1\mu_1 + \mu_2)\tau_{\mu_1+\mu_2}^\dagger, \quad (\text{A.6})$$

$$\mathcal{O}_{\mu_1\mu_2}^{2(+)} = \frac{1}{2}\{\mathcal{O}_{\mu_1\mu_2}^{1(+)}, \tau_0\} = (-1)^{\mu_1}\delta_{\mu_1, -\mu_2}\tau_0, \quad (\text{A.7})$$

$$\mathcal{O}_{\mu_1\mu_2}^{2(-)} = \frac{1}{2}\{\mathcal{O}_{\mu_1\mu_2}^{1(-)}, \tau_0\} = \mu_1\delta_{\mu_1, -\mu_2}, \quad (\text{A.8})$$

$$\mathcal{O}_{\mu_1\mu_2}^{3(\pm)} = \frac{1}{4}(\{\tau_{\mu_1}^\dagger, \mathcal{O}_{\mu_2 0}^{2(+)}\} \pm (\mu_1 \leftrightarrow \mu_2)) = \frac{1}{2}(\delta_{\mu_2, 0}\tau_{\mu_1}^\dagger \pm (\mu_1 \leftrightarrow \mu_2)). \quad (\text{A.9})$$

Accordingly, the isotopic spin dependence of the amplitude is represented by these operators with appropriate spin-spatial amplitudes  $f_l^{(\pm)}$ , where the superscript denotes the symmetry property under interchange of the two pions,

$$t^{\mu_1\mu_2}(\vec{q}_1, \vec{q}_2, \vec{k}) = \sum_{l=1}^3 (f_l^{(+)}(\vec{q}_1, \vec{q}_2, \vec{k})\mathcal{O}_{\mu_1\mu_2}^{l(+)} + f_l^{(-)}(\vec{q}_1, \vec{q}_2, \vec{k})\mathcal{O}_{\mu_1\mu_2}^{l(-)}). \quad (\text{A.10})$$

The functions  $f_l^{(\pm)}$  possess the symmetry property under the exchange of the pion momenta

$$f_l^{(\pm)}(\vec{q}_1, \vec{q}_2, \vec{k}) = \pm f_l^{(\pm)}(\vec{q}_2, \vec{q}_1, \vec{k}). \quad (\text{A.11})$$

The symmetric amplitudes  $f_l^{(+)}$  contribute to the isospin  $T = 0, 2$  part of the  $\pi\pi$  wave function and the antisymmetric ones  $f_l^{(-)}$  to  $T = 1$ . For each diagram in Fig. 1 the dependence on the index  $l$ , i.e. on the operator type, is described by a coefficient so that the functions  $f_l^{(\pm)}$  can be expressed in the simpler form

$$f_l^{(\pm)}(\vec{q}_1, \vec{q}_2, \vec{k}) = C_l^{(\pm)} f^{(\pm)}(\vec{q}_1, \vec{q}_2, \vec{k}), \quad (\text{A.12})$$

where the coefficients  $C_l^{(\pm)}$  are determined by the isotopic structure of the diagram. They are listed in Table IV for the resonance terms as well as for several important Born terms. The amplitudes  $t^{\rho N}$  and  $t^{\sigma N}$  as well as those Born terms, where the pions are produced via the decay of intermediate mesons, contribute either to antisymmetric or symmetric spin-spatial amplitudes only. Thus one has

$$f^{(+/-)}(\vec{q}_1, \vec{q}_2, \vec{k}) = 0, \quad (\text{A.13})$$

for an intermediate  $\rho/\sigma$  meson, respectively. The remaining terms in Fig. 1, contributing, e.g., to  $t^{\pi\Delta}$  in (6), have as a rule mixed spatial symmetry.

For completeness we present also explicit expressions for  $t^{\mu_1\mu_2}$  in terms of the functions  $f_l^{(\pm)}$  for the different charge channels, which can be obtained from (A.5) through (A.10)

$$\begin{aligned} \langle p|t^{1-1}|p\rangle &= -f_1^{(+)} - f_2^{(+)} - f_1^{(-)} + f_2^{(-)}, & \langle n|t^{1-1}|n\rangle &= -f_1^{(+)} + f_2^{(+)} + f_1^{(-)} + f_2^{(-)}, \\ \langle n|t^{10}|p\rangle &= -\frac{1}{\sqrt{2}}(f_3^{(+)} + 2f_1^{(-)} + f_3^{(-)}), & \langle p|t^{-10}|n\rangle &= \frac{1}{\sqrt{2}}(f_3^{(+)} - 2f_1^{(-)} + f_3^{(-)}), \\ \langle p|t^{00}|p\rangle &= \frac{1}{\sqrt{2}}(f_1^{(+)} + f_2^{(+)} + f_3^{(+)}), & \langle n|t^{00}|n\rangle &= \frac{1}{\sqrt{2}}(f_1^{(+)} - f_2^{(+)} - f_3^{(+)}). \end{aligned} \quad (\text{A.14})$$

The expressions for  $\pi^0\pi^0$  photoproduction contain an additional factor  $1/\sqrt{2}$ .

The inverse relations, expressing the amplitudes  $f_i^{(\pm)}$  in terms of the various charge channels, read

$$f_1^{(+)} = \frac{1}{\sqrt{2}}(t_p^{00} + t_n^{00}), \quad (\text{A.15})$$

$$f_2^{(+)} = \frac{1}{2\sqrt{2}}(t^{10} + t^{-10}) - \frac{1}{2}(t_p^{1-1} - t_n^{1-1}), \quad (\text{A.16})$$

$$f_3^{(+)} = \frac{1}{\sqrt{2}}(t_p^{00} - t_n^{00}) - \frac{1}{2\sqrt{2}}(t^{10} + t^{-10}) + \frac{1}{2}(t_p^{1-1} - t_n^{1-1}), \quad (\text{A.17})$$

$$f_1^{(-)} = -\frac{1}{2\sqrt{2}}(t^{10} + t^{-10}), \quad (\text{A.18})$$

$$f_2^{(-)} = \frac{1}{\sqrt{2}}(t_p^{00} + t_n^{00}) + \frac{1}{2}(t_p^{1-1} + t_n^{1-1}), \quad (\text{A.19})$$

$$f_3^{(-)} = \frac{1}{\sqrt{2}}(t^{-10} - t^{10}) - f_3^{(+)}, \quad (\text{A.20})$$

where we have introduced the notation

$$t_{p/n}^{00} := \langle p/n | t^{00} | p/n \rangle, \quad (\text{A.21})$$

$$t_{p/n}^{1-1} := \langle p/n | t^{1-1} | p/n \rangle, \quad (\text{A.22})$$

$$t^{\pm 10} := \langle n/p | t^{\pm 10} | p/n \rangle. \quad (\text{A.23})$$

## APPENDIX B: THE VERTEX FUNCTIONS

Here we give detailed expressions for the isobar vertex functions which determine the various diagrams in Fig. 1. For example, the transition  $\gamma N \rightarrow N^*(\alpha) \rightarrow \pi \Delta \rightarrow \pi N N$  will have the form

$$T = F_{\Delta \rightarrow \pi N} F_{N^*(\alpha) \rightarrow \pi \Delta} G_{\Delta} G_{N^*(\alpha)} F_{\gamma N \rightarrow N^*(\alpha)}, \quad (\text{B.1})$$

where  $F_{\gamma N \rightarrow N^*(\alpha)}$ ,  $F_{N^*(\alpha) \rightarrow \pi \Delta}$  and  $F_{\Delta \rightarrow \pi N}$  denote the appropriate vertex functions for the indicated transitions and  $G_{N^*(\alpha)}$  and  $G_{\Delta}$  the corresponding intermediate dressed resonance propagators. The symbol  $\alpha$  stands for the resonance quantum numbers. In the following, we will characterize a baryon resonance by its total angular momentum  $J$  and its total  $\pi N$  orbital momentum  $L$  instead of its parity, i.e.  $(\alpha) = (J, L)$ .

Before presenting the detailed formalism, we would like to clarify the notation. The vertex functions  $F$  are given in terms of products of irreducible tensors. For the irreducible tensor product we take the usual definition of the coupling of two irreducible tensors

$$[Q^{[j']} \otimes P^{[j]}]_M^{[J]} = \sum_{m'm} (j' m' j m | J M) Q_{m'}^{[j']} P_m^{[j]}, \quad (\text{B.2})$$

where  $(j' m' j m | J M)$  denotes a Clebsch-Gordan coefficient. In particular, the scalar product is related to the tensor product by

$$(Q^{[j]} \cdot P^{[j]}) = (-1)^j \sqrt{2j+1} [Q^{[j]} \otimes P^{[j]}]^{[0]} = \sum_m (-1)^m Q_m^{[j]} P_{-m}^{[j]}. \quad (\text{B.3})$$

For  $j = 1$ , Eq. (B.3) defines the conventional scalar product of two three-vectors given in spherical coordinates, which are defined for a vector  $\vec{q}$  by

$$q_m = \sqrt{\frac{4\pi}{3}} q Y_{1m}(\hat{q}), \quad m = 0, \pm 1. \quad (\text{B.4})$$

For a multiple product, i.e. a repeated coupling of a three-vector  $\vec{Q}$  with itself to the highest possible rank  $l$ , one obtains from (B.3)

$$Q_m^{[l]} \equiv [\dots [[Q^{[1]} \otimes Q^{[1]}]^{[2]} \otimes Q^{[1]}]^{[3]} \dots]_m^{[l]} = \left( \frac{4\pi l!}{(2l+1)!!} \right)^{1/2} Q^l Y_{lm}(\hat{Q}) \quad (\text{B.5})$$

Such multiple products of the type (B.5) appear in the resonance couplings considered below.

Furthermore, for the description of transitions  $N(j = 1/2) \rightarrow N^*(j')/\Delta(j')$  and  $\Delta(j = 3/2) \rightarrow N^*(j')$  one needs in general spin transition operators  $\sigma_{j'j}^{[J]}$ . They are normalized so that the corresponding matrix element is simply given by the associated Clebsch-Gordan coefficient, i.e.

$$\langle j' m' | \sigma_{j'j, M}^{[J]} | j m \rangle = (j m J M | j' m') \quad \text{for } j' \geq j. \quad (\text{B.6})$$

The spin operators for the inverse transitions are then determined by the conjugate operators

$$\sigma_{jj', M}^{[J]} = \sigma_{j'j, M}^{[J]\dagger} = (-1)^M \sigma_{j'j, -M}^{[J]}. \quad (\text{B.7})$$

It should be noted, that the operator  $\sigma_{\frac{1}{2}\frac{1}{2}}$  as defined above is not the ordinary Pauli spin operator but differs from it by a factor  $1/\sqrt{3}$ , namely one finds

$$\langle \frac{1}{2} m' | \sigma_{\frac{1}{2}\frac{1}{2}, M}^{[1]} | \frac{1}{2} m \rangle = (\frac{1}{2} m 1 M | \frac{1}{2} m') = \frac{1}{\sqrt{3}} \sigma_M, \quad (\text{B.8})$$

where  $\sigma_M$  is a spherical component of the Pauli spin matrix.

Now we will consider the e.m. vertex functions possessing electric and magnetic couplings. They can be presented in the general form

$$F_{\gamma N \rightarrow N^*(J, L)}^E = \frac{g^E}{2M_N^{j-1}} (\sigma_{J, \frac{1}{2}}^{[j]} \cdot [k^{[j-1]} \otimes \epsilon^{[1]}]^{[j]}), \quad j = 2J - L, \quad (\text{B.9})$$

$$F_{\gamma N \rightarrow N^*(J, L)}^M = \frac{g^M}{2M_N^j} (\sigma_{J, \frac{1}{2}}^{[j]} \cdot [k^{[j]} \otimes \epsilon^{[1]}]^{[j]}), \quad j = L, \quad (\text{B.10})$$

where  $\vec{k}$  denotes the photon momentum, and the rank of the multipole  $j$  is fixed by the parity of the transition. For each resonance the values of  $j$  are given in the last column of Table I. In order to fix the constants  $g^E$  and  $g^M$ , we use the helicity amplitudes listed in [11]. They are related to the vertices in (B.9) and (B.10) by

$$A_\lambda(J, L) = \frac{1}{\sqrt{2}\omega_\gamma} \langle N^*; J, \lambda | F_{\gamma N \rightarrow N^*(J, L)}^E + F_{\gamma N \rightarrow N^*(J, L)}^M | N; \frac{1}{2}, \lambda - 1; \gamma; (\lambda_\gamma = 1) \rangle, \quad \lambda = \frac{1}{2}, \frac{3}{2}. \quad (\text{B.11})$$

The electromagnetic width of the decay of a resonance  $N^*(J, L)$  into a nucleon then is

$$\Gamma_{N^*(J, L) \rightarrow \gamma N} = \frac{2M_N \omega_\gamma^2}{\pi(2J+1)M_{N^*}} (|A_{1/2}(J, L)|^2 + |A_{3/2}(J, L)|^2) = \Gamma_{\gamma N^*}^{1/2}(W) + \Gamma_{\gamma N^*}^{3/2}(W). \quad (\text{B.12})$$

From Eq. (B.11) one obtains the following expressions relating the constants  $g^{E(M)}$  to the helicity amplitudes  $A_\lambda$

$$A_\lambda(J, L) = \frac{1}{4\sqrt{\omega_\gamma}} \left( \frac{\omega_\gamma}{M_N} \right)^L \sqrt{\frac{L!}{(2L+1)!!}} \left[ -2(1-\lambda) \sqrt{\frac{(L+2)(L+3-2\lambda)}{2L+3}} g^E + \sqrt{L-1+2\lambda} g^M \right], \quad (\text{B.13})$$

for  $J = L + 1/2$ , and

$$A_\lambda(J, L) = \frac{1}{4\sqrt{\omega_\gamma}} \left( \frac{\omega_\gamma}{M_N} \right)^{L-2} \sqrt{\frac{L!}{(2L+1)!!}} \left[ \sqrt{\frac{(2L+1)(L-2+2\lambda)}{L-1}} g^E - 2(1-\lambda) \sqrt{L+2-2\lambda} \left( \frac{\omega_\gamma}{M_N} \right)^2 g^M \right], \quad (\text{B.14})$$

for  $J = L - 1/2$ . The electromagnetic coupling constants calculated according to these formulae at the resonance position  $\omega_\gamma^* = (M_{N^*}^2 - M_N^2)/2M_{N^*}$  are given in Table II. For resonances with isospin  $T = 1/2$ , they are split into isoscalar and isovector parts, i.e.

$$g_{p/n} = g^{(s)} \pm g^{(v)}. \quad (\text{B.15})$$

As next we will consider the meson-baryon vertices denoting always the meson momentum by  $\vec{q}$ . The  $\pi N$  vertices can be presented in the general form as

$$F_{N^*(J, L) \rightarrow \pi N} = -i \frac{f_{N^* \pi N}}{m_\pi^L} (\sigma_{\frac{1}{2}, J}^{[L]} \cdot q^{[L]}), \quad (\text{B.16})$$

and those for  $\sigma N$  read

$$F_{N^*(J,L)\rightarrow\sigma N} = \frac{f_{N^*\sigma N}}{m_\sigma^l} (\sigma_{\frac{1}{2},J}^{[l]} \cdot q^{[l]}), \quad (\text{B.17})$$

where  $l - L \equiv 1 \pmod{2}$ . For the  $N^* \rightarrow \pi\Delta$  decay vertex we have

$$F_{N^*(J,L)\rightarrow\pi\Delta} = \sum_{\substack{l=|J-3/2| \\ l \equiv L \pmod{2}}}^{J+3/2} -i \frac{f_{N^*\pi\Delta}}{m_\pi^l} (\sigma_{\frac{3}{2},J}^{[l]} \cdot q^{[l]}). \quad (\text{B.18})$$

Because of the delta spin 3/2 the pion angular momentum  $l$  in (B.18) is not fixed by the angular momentum  $L$  of the resonance. But its possible variation is of course restricted by parity conservation. For the actual calculation, only in the case of  $D_{13}(1520)$  we have taken into account both, the  $l = 0$  and  $l = 2$  waves. For other resonances with  $J \geq \frac{3}{2}$ , where the particle data listings [11] do not give definite contributions from different waves, only the lowest possible value of  $l$  is taken.

The  $N^* \rightarrow \rho N$  vertex functions has a more complicated structure

$$F_{N^*(J,L)\rightarrow\rho N} = \sum_{j=|J-\frac{1}{2}|}^{J+\frac{1}{2}} \sum_{l=|j-1|}^{j+1} \frac{f_{N^*\rho N}}{m_\rho^l} (\sigma_{\frac{1}{2},J}^{[j]} \cdot [q^{[l]} \otimes \epsilon_\rho^{[1]}]^{[j]}), \quad (\text{B.19})$$

where the orbital momentum  $l$  of the  $\rho$  meson is even for  $N^*$  with negative parity and odd for positive parity. Again only the lowest possible values of  $j$  and  $l$  were used in the calculation. Explicit expressions for the various vertices  $F_{N^*(J,L)\rightarrow X}$  are listed in Table IV.

Each resonance hadronic vertex contains a form factor of the form

$$F_r(Q^2) = \frac{\Lambda_r^4}{\Lambda_r^4 - (Q^2 - M_r^2)^2}, \quad (\text{B.20})$$

where  $Q^2$  and  $M_r$  denote squared four-momentum and mass of the resonance, respectively. For all resonances we take  $\Lambda_r = 1.3$  GeV. The same form factors were used for meson exchange in the  $t$  channel (diagrams (2),(5)-(7), and (9)-(10) of Fig. 1). For the  $\pi NN$  vertex, we taken the familiar dipole form factor

$$F_{\pi NN}(q^2) = \frac{\Lambda^2}{\Lambda^2 + q^2} \quad (\text{B.21})$$

with  $\Lambda = 0.8$  GeV. For the decays of  $\rho$  and  $\sigma$  mesons the following couplings were used

$$\begin{aligned} F_{\rho\rightarrow\pi\pi}^{(j=1,\mu)} &= -f_{\rho\pi\pi} \epsilon_\rho^\mu \cdot (\vec{q}_1 - \vec{q}_2), & \frac{f_{\rho\pi\pi}^2}{4\pi} &= \frac{3}{2} \frac{m_\rho^2}{q^{*3}} \Gamma_{\rho\rightarrow\pi\pi}, \\ F_{\sigma\rightarrow\pi\pi}^{(j=0)} &= -2m_\sigma f_{\sigma\pi\pi}, & \frac{f_{\sigma\pi\pi}^2}{4\pi} &= \frac{1}{2q^*} \Gamma_{\sigma\rightarrow\pi\pi}, \end{aligned} \quad (\text{B.22})$$

with  $q^*$  being the  $\pi\pi$  c.m. momentum at  $\omega_{\pi\pi} = m_\mu$ , ( $\mu \in \{\rho, \sigma\}$ ). Finally the resonance propagators were taken in the form

$$G_{N^*}(W) = [W - M_{N^*} + \frac{i}{2} \Gamma_{N^*}(W)]^{-1}, \quad (\text{B.23})$$

$$G_\mu(W) = [W^2 - m_\mu^2 + im_\mu \Gamma_\mu(W)]^{-1}, \quad \mu \in \{\rho, \sigma\}. \quad (\text{B.24})$$

For completeness we present also the expressions for the resonance widths, in order to fix the normalization of the hadronic coupling constants. For the two-body  $\pi N$  decay one has

$$\Gamma_{N^*(J,L)\rightarrow\pi N}(W) = (2\pi)^4 \frac{1}{2J+1} \int \frac{d^3p}{(2\pi)^3} \frac{M_N}{E_N} \frac{d^3q}{2\omega(2\pi)^3} \delta(W - \omega - E_N) \delta^{(3)}(\vec{q} + \vec{p}) \sum_{m_j m} |\langle \frac{1}{2} m | F_{N^*\rightarrow\pi N} | J m_J \rangle|^2. \quad (\text{B.25})$$

With the help of (B.16) one obtains

$$\Gamma_{N^*(J,L)\rightarrow\pi N}(W) = \frac{f_{N^*\pi N}^2}{4\pi} \frac{2M_N}{W m_\pi^{2L}} \frac{L!}{(2L+1)!} q^{2L+1} \quad (\text{B.26})$$

with the pion momentum in the  $\pi N$  c.m. frame

$$q = \frac{\sqrt{\lambda(W, M_N, m_\pi)}}{2W}, \quad (\text{B.27})$$

where  $\lambda(\alpha, \beta, \gamma) = ((\alpha + \beta)^2 - \gamma^2)((\alpha - \beta)^2 - \gamma^2)$ . For the decay into the  $\pi\pi N$  channel we assume a sequential decay mechanism via an intermediate  $\pi\Delta$  channel. Then one finds for the decay width, indicating by the superscript  $(\pi\Delta)$  the intermediate channel in the sequential mechanism,

$$\begin{aligned} \Gamma_{N^*(J,L) \rightarrow \pi\pi N}^{(\pi\Delta)}(W) &= (2\pi)^4 \frac{1}{2J+1} \int \frac{M_N}{E_N} \frac{d^3 p}{(2\pi)^3} \frac{d^3 q_1}{2\omega_1 (2\pi)^3} \frac{d^3 q_2}{2\omega_2 (2\pi)^3} \delta(W - \omega_1 - \omega_2 - E_N) \\ &\quad \times \delta^{(3)}(\vec{q}_1 + \vec{q}_2 + \vec{p}) \sum_{m_J m_\Delta} \left| \sum_{m_\Delta} \langle \frac{1}{2} m | F_{\Delta \rightarrow \pi N} | \frac{3}{2} m_\Delta \rangle G_\Delta(w_\Delta) \langle \frac{3}{2} m_\Delta | F_{N^* \rightarrow \pi \Delta} | J m_J \rangle \right|^2 \\ &= \frac{1}{2\pi W} \frac{1}{2J+1} \int_{M_N+m_\pi}^{W-m_\pi} dw_\Delta w_\Delta q(w_\Delta) \rho(w_\Delta) \sum_{m_J m_\Delta} \left| \langle \frac{3}{2} m_\Delta | F_{N^* \rightarrow \pi \Delta} | J m_J \rangle \right|^2, \end{aligned} \quad (\text{B.28})$$

with

$$q(w_\Delta) = \frac{\sqrt{\lambda(W, w_\Delta, m_\pi)}}{2W} \quad \text{and} \quad \rho(w_\Delta) = \frac{1}{2\pi} \Gamma_\Delta(w_\Delta) |G_\Delta(w_\Delta)|^2, \quad (\text{B.29})$$

where  $\Gamma_\Delta$  denotes the width of the  $\Delta$  resonance. The final expression is formally equal to (B.26)

$$\Gamma_{N^*(J,L) \rightarrow \pi\pi N}^{(\pi\Delta)}(W) = \sum_{\substack{l=|J-3/2| \\ l \equiv L \pmod{2}}}^{|J+3/2|} \frac{f_{N^* \pi \Delta}^{(l)2}}{4\pi} \frac{2M_\Delta}{W m_\Delta^{2l}} \frac{l!}{(2l+1)!!} \bar{q}^{2l+1}, \quad (\text{B.30})$$

but where

$$\bar{q}^{2l+1} = \int_{M_N+m_\pi}^{W-m_\pi} \frac{w_\Delta dw_\Delta}{M_\Delta} q(w_\Delta)^{2l+1} \rho(w_\Delta). \quad (\text{B.31})$$

For the other type of sequential decay  $N^* \rightarrow \mu N \rightarrow \pi\pi N$  with  $\mu \in \{\rho, \sigma\}$  one has, denoting the spin of the meson by  $j_\mu$ ,

$$\begin{aligned} \Gamma_{N^*(J,L) \rightarrow \pi\pi N}^{(\mu N)}(W) &= (2\pi)^4 \frac{1}{2J+1} \int \frac{M_N}{E_N} \frac{d^3 p}{(2\pi)^3} \frac{d^3 q_1}{2\omega_1 (2\pi)^3} \frac{d^3 q_2}{2\omega_2 (2\pi)^3} \delta(W - \omega_1 - \omega_2 - E_N) \\ &\quad \times \delta^{(3)}(\vec{q}_1 + \vec{q}_2 + \vec{p}) \sum_{m_J, m} \left| \sum_{m'} \langle J m_J | F_{N^* \rightarrow \mu N} | \frac{1}{2} m; j_\mu m' \rangle G_\mu(w_{\pi\pi}) F_{\mu \rightarrow \pi\pi}^{(j_\mu, m')} \right|^2 \\ &= \frac{1}{2\pi} \frac{M_N}{W} \frac{1}{2J+1} \int_{2m_\pi}^{W-M_N} dw_{\pi\pi} q(w_{\pi\pi}) \rho(w_{\pi\pi}) \sum_{m_J, m, m'} \left| \langle J m_J | F_{N^* \rightarrow \mu N} | \frac{1}{2} m; j_\mu, m' \rangle \right|^2. \end{aligned} \quad (\text{B.32})$$

with

$$q(w_{\pi\pi}) = \frac{\sqrt{\lambda(W, w_{\pi\pi}, M_N)}}{2W} \quad \text{and} \quad \rho(w_{\pi\pi}) = \frac{1}{2\pi} 4m_\mu w_{\pi\pi} \Gamma_\mu(w_{\pi\pi}) |G_\mu(w_{\pi\pi})|^2. \quad (\text{B.33})$$

Then one has as final result

$$\Gamma_{N^*(J,L) \rightarrow \pi\pi N}^{(\mu N)}(W) = \sum_{\substack{l=l_{\min} \\ l \equiv L+j_\mu+1 \pmod{2}}}^{J+j_\mu+1/2} \frac{f_{N^* \mu N}^{(l)2}}{4\pi} \frac{2M_N}{W m_\mu^{2l}} \frac{l!}{(2l+1)!!} \bar{q}^{2l+1}, \quad (\text{B.34})$$

where  $l_{\min} = \min(|J - |j_\mu - 1/2||, |J - |j_\mu + 1/2||)$  and

$$\bar{q}^{2l+1} = \int_{2m_\pi}^{W-M_N} q^{2l+1}(w_{\pi\pi}) \rho(w_{\pi\pi}) dw_{\pi\pi}. \quad (\text{B.35})$$

The values of the hadronic coupling constants calculated with the help of (B.26), (B.30), and (B.34) and partial decay widths from [11] are listed in Tables II and III.

### APPENDIX C: THE AMPLITUDES

In this appendix we present detailed expressions for the amplitudes associated with the resonance terms (diagrams (18)-(20) of Fig. 1) and those background diagrams that are important in the second resonance region. Since the isospin part is considered in Appendix A, we list here only the corresponding spin structures, namely the functions  $f^{(\pm)}(\vec{q}_1, \vec{q}_2, \vec{k})$  appearing in (A.12). The amplitudes  $f^{(\pm)}$  are presented in the form of Eq. (4), i.e. by listing  $K^{(\pm)}$  and  $\vec{L}^{(\pm)}$  of the general form

$$f^{(\pm)} = A \left( K^{(\pm)} + i\vec{\sigma} \cdot \vec{L}^{(\pm)} \right). \quad (\text{C.1})$$

The momenta of the participating particles are already defined in (1). For convenience we introduce in addition a set of relative momenta  $\vec{p}_i$  as follows:

(i) The relative momentum between  $\pi_1$  and the total momentum of the  $\pi_2 N_f$  subsystem

$$\vec{p}_1 = \frac{\vec{q}_1(E_f + \omega_2) - (\vec{q}_2 + \vec{p}_f)\omega_1}{E_f + \omega_1 + \omega_2} = \vec{q}_1 - \frac{\omega_1}{\omega_\gamma + E_i}(\vec{k} + \vec{p}_i), \quad (\text{C.2})$$

(ii) the relative momentum between  $\pi_2$  and the final nucleon  $N_f$

$$\vec{p}_2 = \frac{\vec{q}_2 E_f - \vec{p}_f \omega_2}{E_f + \omega_2} = \vec{q}_2 - \frac{\omega_2}{E_f + \omega_2}(\vec{q}_2 + \vec{p}_f). \quad (\text{C.3})$$

The argument  $\omega_{\pi_i N}$  of the  $\Delta$ -propagator denotes the invariant mass of the  $\pi_i N$  subsystem. To make the formulae more compact we use the following notations for scalar and vector products

$$(ab) = (\vec{a} \cdot \vec{b}), \quad [ab] = (\vec{a} \times \vec{b}). \quad (\text{C.4})$$

The resonance coupling constants are listed in Tables II and III. Other constants are given together with corresponding formulas.

1.  $\Delta$  Kroll-Ruderman (diagram (8)):

$$\begin{aligned} \vec{L}^{(\pm)} &= [p_2 \epsilon] G_\Delta(w_{\pi_2 N}) \pm (1 \leftrightarrow 2), \\ K^{(\pm)} &= -(p_2 \epsilon) G_\Delta(w_{\pi_2 N}) \pm (1 \leftrightarrow 2), \\ A &= \frac{e}{3} \left( \frac{f_{\Delta \pi N}}{m_\pi} \right)^2. \end{aligned}$$

2.  $N\Delta$  u-channel term (the second diagram from the group (12), M1  $N \rightarrow \Delta$  transition):

$$\begin{aligned} \vec{L}^{(\pm)} &= \left[ 2(q_1 p_2)[k\epsilon] - (p_2 \epsilon)[q_1 k] + (p_2 k)[q_1 \epsilon] + 2(q_1 \epsilon)[p_2 k] \right. \\ &\quad \left. - 2(q_1 k)[p_2 \epsilon] \right] G_\Delta(w_{\pi_2 N}) \left( E_i - \omega_1 - \sqrt{(\vec{p}_i - \vec{q}_1)^2 + M_N^2} \right)^{-1} \pm (1 \leftrightarrow 2), \\ K^{(\pm)} &= \left[ (q_1 k)(p_2 \epsilon) - (p_2 k)(q_1 \epsilon) \right] G_\Delta(w_{\pi_2 N}) \left( E_i - \omega_1 - \sqrt{(\vec{p}_i - \vec{q}_1)^2 + M_N^2} \right)^{-1} \pm (1 \leftrightarrow 2), \\ A &= -\frac{g^M f_{\Delta \pi N} f_{\pi NN}}{12\sqrt{2}M_N m_\pi^2}, \\ g^M &= -1.845, \quad f_{\pi NN} = 1.0 \end{aligned}$$

3.  $\Delta\Delta$  u-channel term (the second diagram from the group (14), M1  $\Delta \rightarrow \Delta$  transition):

$$\begin{aligned} \vec{L}^{(\pm)} &= \left[ 2(q_1 p_2)[k\epsilon] - (p_2 \epsilon)[q_1 k] + (p_2 k)[q_1 \epsilon] - (q_1 \epsilon)[p_2 k] \right. \\ &\quad \left. + (q_1 k)[p_2 \epsilon] \right] G_\Delta(w_{\pi_2 N}) \left( E_i - \omega_1 - \sqrt{(\vec{p}_i - \vec{q}_1)^2 + M_\Delta^2} \right)^{-1} \pm (1 \leftrightarrow 2), \\ K^{(\pm)} &= 5 \left[ -(q_1 k)(p_2 \epsilon) + (p_2 k)(q_1 \epsilon) \right] G_\Delta(w_{\pi_2 N}) \left( E_i - \omega_1 - \sqrt{(\vec{p}_i - \vec{q}_1)^2 + M_\Delta^2} \right)^{-1} \pm (1 \leftrightarrow 2), \\ A &= \frac{e\mu_p}{36M_N} \left( \frac{f_{\Delta \pi N}}{m_\pi} \right)^2, \\ \mu_p &= 2.79 \end{aligned}$$

4.  $\rho$  Kroll-Ruderman term (diagram(4)):

$$\begin{aligned}\vec{L}^{(-)} &= [q_2\epsilon] - [q_1\epsilon], \quad \vec{L}^{(+)} = 0, \\ K^{(\pm)} &= 0, \\ A &= e(1 + \kappa_\rho) \frac{f_{\rho NN}}{2M_N} f_{\rho\pi\pi} G_\rho(w_{\pi\pi}), \\ f_{\rho NN} &= 2.24, \quad \kappa_\rho = 6, \quad f_{\rho\pi\pi} = 6.02.\end{aligned}$$

5.  $\rho$  photoproduction via  $\sigma$  exchange (diagram(6)):

$$\begin{aligned}\vec{L}^{(\pm)} &= 0, \\ K^{(-)} &= (q_1\epsilon)\omega_\gamma(\omega_1 + \omega_2) + 2(q_2\epsilon)(q_1k) - (1 \leftrightarrow 2), \\ K^{(+)} &= 0, \\ A &= -e \frac{f_{\gamma\rho\sigma}}{m_\rho} \frac{f_{\sigma NN} f_{\rho\pi\pi}}{t - m_\sigma^2} G_\rho(w_{\pi\pi}), \\ f_{\gamma\rho\sigma} &= 2.2, \quad f_{\sigma NN} = 10.02.\end{aligned}$$

6.  $\gamma(E1)N \rightarrow N^*(\frac{1}{2}, 0) \rightarrow \pi\Delta$ :

$$\begin{aligned}\vec{L}^{(\pm)} &= \left[ (p_1 p_2) [p_1\epsilon] - \frac{1}{3} p_1^2 [p_2\epsilon] \right] G_\Delta(w_{\pi_2 N}) \pm (1 \leftrightarrow 2), \\ K^{(\pm)} &= \left[ (p_1 p_2) (p_1\epsilon) - \frac{1}{3} p_1^2 (p_2\epsilon) \right] G_\Delta(w_{\pi_2 N}) \pm (1 \leftrightarrow 2), \\ A &= -\frac{f_{N^*\pi\Delta} f_{\Delta\pi N}}{2\sqrt{30} m_\pi^3} G_{N^*}(W).\end{aligned}$$

7.  $\gamma(E1)N \rightarrow N^*(\frac{1}{2}, 0) \rightarrow \rho N$ :

$$\begin{aligned}\vec{L}^{(-)} &= [p_1\epsilon] - [p_2\epsilon], \quad \vec{L}^{(+)} = 0, \\ K^{(-)} &= (p_1\epsilon) - (p_2\epsilon), \quad K^{(+)} = 0, \\ A &= -\frac{1}{6} f_{N^*\rho N} f_{\rho\pi\pi} G_{N^*}(W) G_\rho(w_{\pi\pi}).\end{aligned}$$

8.  $\gamma(E1)N \rightarrow N^*(\frac{1}{2}, 0) \rightarrow \sigma N$ :

$$\begin{aligned}\vec{L}^{(+)} &= [p_1\epsilon] + [p_2\epsilon], \quad \vec{L}^{(-)} = 0, \\ K^{(+)} &= (p_1\epsilon) + (p_2\epsilon), \quad K^{(-)} = 0, \\ A &= -\frac{1}{3} f_{N^*\sigma N} f_{\sigma\pi\pi} G_{N^*}(W) G_\sigma(w_{\pi\pi}).\end{aligned}$$

9.  $\gamma(M1)N \rightarrow N^*(\frac{1}{2}, 1) \rightarrow \pi\Delta$ :

$$\begin{aligned}\vec{L}^{(-)} &= \left[ (p_2 k) [p_1\epsilon] + (p_1\epsilon) [p_2 k] \right] G_\Delta(w_{\pi_2 N}) - (1 \leftrightarrow 2), \\ \vec{L}^{(+)} &= (p_1 p_2) [k\epsilon] G_\Delta(w_{\pi_2 N}) + (1 \leftrightarrow 2), \\ K^{(-)} &= (p_2 k) (p_1\epsilon) G_\Delta(w_{\pi_2 N}) - (1 \leftrightarrow 2), \quad K^{(+)} = 0, \\ A &= -\frac{f_{N^*\pi\Delta} f_{\Delta\pi N}}{6\sqrt{6} M_N m_\pi^2} G_{N^*}(W).\end{aligned}$$

10.  $\gamma(M1)N \rightarrow N^*(\frac{1}{2}, 1) \rightarrow \sigma N$ :

$$\begin{aligned}\vec{L}^{(+)} &= [k\epsilon], \quad \vec{L}^{(-)} = 0, \\ K^{(\pm)} &= 0, \\ A &= -\frac{m_\sigma f_{N^*\sigma N} f_{\sigma\pi\pi}}{\sqrt{6} M_N} G_{N^*}(W) G_\sigma(w_{\pi\pi}).\end{aligned}$$



11.  $\gamma(E1)N \rightarrow N^* \left(\frac{3}{2}, 2\right) \rightarrow \pi\Delta$ :

$$\begin{aligned}\vec{L}^{(\pm)} &= \left[ -\frac{f_{N^*\pi\Delta}^{(s)}}{2}[p_2\epsilon] - \sqrt{\frac{6}{5}}\frac{f_{N^*\pi\Delta}^{(d)}}{2m_\pi^2}([p_1p_2](p_1\epsilon) - (p_1p_2)[p_1\epsilon] + \frac{2}{3}p_1^2[p_2\epsilon]) \right] G_\Delta(w_{\pi_2N}) \pm (1 \leftrightarrow 2), \\ K^{(\pm)} &= \left[ f_{N^*\pi\Delta}^{(s)}(p_2\epsilon) - \sqrt{\frac{6}{5}}\frac{f_{N^*\pi\Delta}^{(d)}}{2m_\pi^2}((p_1p_2)(p_1\epsilon) - \frac{1}{3}p_1^2(p_2\epsilon)) \right] G_\Delta(w_{\pi_2N}) \pm (1 \leftrightarrow 2), \\ A &= -\frac{f_{\Delta\pi N}}{6m_\pi} G_{N^*}(W).\end{aligned}$$

12.  $\gamma(M2)N \rightarrow N^* \left(\frac{3}{2}, 2\right) \rightarrow \pi\Delta$ :

$$\begin{aligned}\vec{L}^{(\pm)} &= \left[ \frac{f_{N^*\pi\Delta}^{(s)}}{2}(2(p_2k)[k\epsilon] - k^2[p_2\epsilon]) \right. \\ &\quad - \sqrt{\frac{6}{5}}\frac{f_{N^*\pi\Delta}^{(d)}}{6m_\pi^2}([k\epsilon]\{3(p_1k)(p_1p_2) - p_1^2(p_2k)\} + [p_2k](p_1k)(p_1\epsilon) \\ &\quad + [p_1\epsilon]\{(p_1k)(p_2k) - 2(p_1p_2)k^2\} + [p_2\epsilon]\{p_1^2k^2 - (p_1k)^2\} \\ &\quad \left. - [p_1k]\{2(p_1k)(p_2\epsilon) - (p_1\epsilon)(p_2k)\}) \right] G_\Delta(w_{\pi_2N}) \pm (1 \leftrightarrow 2), \\ K^{(\pm)} &= \sqrt{\frac{6}{5}}\frac{f_{N^*\pi\Delta}^{(d)}}{6m_\pi^2} \left[ 2(p_1k)^2(p_2\epsilon) - 2(p_1k)(p_1\epsilon)(p_2k) - k^2p_1^2(p_2\epsilon) + k^2(p_1\epsilon)(p_1p_2) \right] G_\Delta(w_{\pi_2N}) \pm (1 \leftrightarrow 2), \\ A &= -\frac{f_{\Delta\pi N}}{2\sqrt{15}M_N^2m_\pi} G_{N^*}(W).\end{aligned}$$

13.  $\gamma(E1)N \rightarrow N^* \left(\frac{3}{2}, 2\right) \rightarrow \rho N$ :

$$\begin{aligned}\vec{L}^{(-)} &= [p_2\epsilon] - [p_1\epsilon], \quad \vec{L}^{(+)} = 0, \\ K^{(-)} &= 2(p_1\epsilon) - 2(p_2\epsilon), \quad K^{(+)} = 0, \\ A &= -\frac{1}{6}f_{N^*\rho N}f_{\rho\pi\pi}G_{N^*}(W)G_\rho(w_{\pi\pi}).\end{aligned}$$

14.  $\gamma(M2)N \rightarrow N \left(\frac{3}{2}, 2\right) \rightarrow \rho N$ :

$$\begin{aligned}\vec{L}^{(-)} &= 2[k\epsilon](p_1k) - k^2[p_1\epsilon] - (1 \leftrightarrow 2), \quad \vec{L}^{(+)} = 0, \\ K^{(\pm)} &= 0, \\ A &= -\frac{f_{N^*\rho N}f_{\rho\pi\pi}}{2\sqrt{15}M_N^2} G_{N^*}(W)G_\rho(w_{\pi\pi}).\end{aligned}$$

15.  $\gamma(M1)N \rightarrow N \left(\frac{3}{2}, 1\right) \rightarrow \pi\Delta$ :

$$\begin{aligned}\vec{L}^{(-)} &= \frac{5}{2}[(p_2k)[p_1\epsilon] - (p_2\epsilon)[p_1k]] G_\Delta(w_{\pi_2N}) - (1 \leftrightarrow 2), \\ \vec{L}^{(+)} &= \left[ (p_1p_2)[k\epsilon] + \frac{3}{2}((p_2\epsilon)[p_1k] - (p_2k)[p_1\epsilon]) \right] G_\Delta(w_{\pi_2N}) + (1 \leftrightarrow 2), \\ K^{(-)} &= 5(p_1k)(p_2\epsilon)G_\Delta(w_{\pi_2N}) - (1 \leftrightarrow 2), \quad K^{(+)} = 0, \\ A &= -\frac{f_{N^*\pi\Delta}f_{\Delta\pi N}}{6\sqrt{30}M_Nm_\pi^2} G_{N^*}(W).\end{aligned}$$

16.  $\gamma(E2)N \rightarrow N^* \left(\frac{3}{2}, 1\right) \rightarrow \rho N$ :

$$\begin{aligned}\vec{L}^{(-)} &= (p_1\epsilon)[p_2k] + (p_1k)[p_2\epsilon] - (1 \leftrightarrow 2), \quad \vec{L}^{(+)} = 0, \\ K^{(\pm)} &= 0, \\ A &= \frac{f_{N^*\rho N}f_{\rho\pi\pi}}{2\sqrt{5}m_\rho M_N} G_{N^*}(W)G_\rho(w_{\pi\pi}).\end{aligned}$$

17.  $\gamma(M1)N \rightarrow N^* \left(\frac{3}{2}, 2\right) \rightarrow \rho N$ :

$$\begin{aligned}\vec{L}^{(-)} &= (p_2 k)[p_1 \epsilon] + (p_1 \epsilon)[p_2 k] - (1 \leftrightarrow 2), \quad \vec{L}^{(+)} = 0, \\ K^{(-)} &= 2(p_1 k)(p_2 \epsilon) - (1 \leftrightarrow 2), \quad K^{(+)} = 0, \\ A &= -\frac{f_{N^* \rho N} f_{\rho \pi \pi}}{6 m_\rho M_N} G_{N^*}(W) G_\rho(w_{\pi \pi}).\end{aligned}$$

18.  $\gamma(E3)N \rightarrow N^* \left(\frac{5}{2}, 2\right) \rightarrow \pi \Delta$ :

$$\begin{aligned}\vec{L}^{(\pm)} &= \left[ [p_1 \epsilon](-10k^2(p_1 p_2) + 22(p_1 k)(p_2 k)) + [p_1 k](8(p_1 \epsilon)(p_2 k) + 15(p_2 \epsilon)(p_1 k)) \right. \\ &\quad \left. + [p_2 \epsilon](9p_1^2 k^2 - 17(p_1 k)^2) - 13[p_2 k](p_1 \epsilon)(p_1 k) + 7[k \epsilon]((p_1 p_2)(p_1 k) \right. \\ &\quad \left. - p_1^2(p_2 k)) \right] G_\Delta(w_{\pi_2 N}) \pm (1 \leftrightarrow 2), \\ K^{(\pm)} &= \left[ 2(p_1 \epsilon)(5(p_1 k)(p_2 k) - (p_1 p_2)k^2) + (p_2 \epsilon)(5(p_1 k)^2 - p_1^2 k^2) \right] G_\Delta(w_{\pi_2 N}) \pm (1 \leftrightarrow 2), \\ A &= -\frac{\sqrt{2}}{105} \frac{f_{N^* \pi \Delta} f_{\Delta \pi N}}{4 M_N^2 m_\pi^3} G_{N^*}(W).\end{aligned}$$

19.  $\gamma(M2)N \rightarrow N^* \left(\frac{5}{2}, 2\right) \rightarrow \pi \Delta$ :

$$\begin{aligned}\vec{L}^{(\pm)} &= \frac{1}{7} \left[ -[p_1 \epsilon](k^2(p_1 p_2) + 2(p_1 k)(p_2 k)) + 2[p_1 k](4(p_1 \epsilon)(p_2 k) - 3(p_2 \epsilon)(p_1 k)) \right. \\ &\quad \left. + [p_2 \epsilon](3p_1^2 k^2 - 8(p_1 k)^2) + 8[p_2 k](p_1 \epsilon)(p_1 k) + 2[k \epsilon](2(p_1 p_2)(p_1 k) + p_1^2(p_2 k)) \right] G_\Delta(w_{\pi_2 N}) \pm (1 \leftrightarrow 2), \\ K^{(\pm)} &= \left[ (p_1 \epsilon)(k^2(p_1 p_2) - 2(p_1 k)(p_2 k)) + (p_2 \epsilon)(2(p_1 k)^2 - p_1^2 k^2) \right] G_\Delta(w_{\pi_2 N}) \pm (1 \leftrightarrow 2), \\ A &= -\frac{\sqrt{7}}{15} \frac{f_{N^* \pi \Delta} f_{\Delta \pi N}}{4 M_N^2 m_\pi^3} G_{N^*}(W).\end{aligned}$$

20.  $\gamma(E2)N \rightarrow N^* \left(\frac{5}{2}, 3\right) \rightarrow \pi \Delta$ :

$$\begin{aligned}\vec{L}^{(+)} &= \left[ -(p_2 k)[p_1 \epsilon] - (p_2 \epsilon)[p_1 k] \right] G_\Delta(w_{\pi_2 N}) + (1 \leftrightarrow 2), \quad \vec{L}^{(-)} = 0, \\ K^{(+)} &= 3(p_2 k)(p_1 \epsilon) G_\Delta(w_{\pi_2 N}) + (1 \leftrightarrow 2), \quad K^{(-)} = 0, \\ A &= -\frac{1}{10} \frac{f_{N^* \pi \Delta} f_{\Delta \pi N}}{2 M_N m_\pi^2} G_{N^*}(W).\end{aligned}$$

21.  $\gamma(M3)N \rightarrow N \left(\frac{5}{2}, 3\right) \rightarrow \pi \Delta$ :

$$\begin{aligned}\vec{L}^{(+)} &= \left[ k^2(4(p_2 k)[p_1 \epsilon] + (p_2 \epsilon)[p_1 k]) + \frac{3}{2}[k \epsilon](p_1 p_2) - \frac{15}{2}[k \epsilon](p_1 k)(p_2 k) \right] G_\Delta(w_{\pi_2 N}) + (1 \leftrightarrow 2), \\ \vec{L}^{(-)} &= 0, \\ K^{(\pm)} &= 0, \\ A &= \frac{1}{10\sqrt{7}} \frac{f_{N^* \pi \Delta} f_{\Delta \pi N}}{2 M_N^3 m_\pi^2} G_{N^*}(W).\end{aligned}$$

22.  $\gamma(E2)N \rightarrow N \left(\frac{5}{2}, 3\right) \rightarrow \rho N$ :

$$\begin{aligned}\vec{L}^{(-)} &= (p_1 k)[p_1 \epsilon] + (p_1 \epsilon)[p_1 k] - (1 \leftrightarrow 2), \quad \vec{L}^{(+)} = 0, \\ K^{(-)} &= 3(p_2 \epsilon)(p_2 k) - (1 \leftrightarrow 2), \quad K^{(+)} = 0, \\ A &= \frac{1}{5} \frac{f_{N^* \rho N} f_{\rho \pi \pi}}{2 M_N m_\rho} G_{N^*}(W) G_\rho(w_{\pi \pi}).\end{aligned}$$

23.  $\gamma(M3)N \rightarrow N(\frac{5}{2}, 3) \rightarrow \rho N$ :

$$\begin{aligned}\vec{L}^{(-)} &= k^2(4(p_1k)[p_1\epsilon] + (p_1\epsilon)[p_1k] + \frac{3}{4}(p_1^2 - p_2^2)[k\epsilon]) - \frac{15}{4}[k\epsilon]((p_1k)^2 - (p_2k)^2) - (1 \leftrightarrow 2), \\ \vec{L}^{(+)} &= 0, \\ K^{(\pm)} &= 0, \\ A &= \frac{1}{5\sqrt{7}} \frac{f_{N^*\rho N} f_{\rho\pi\pi}}{2M_N^3 m_\rho} G_{N^*}(W) G_\rho(w_{\pi\pi}).\end{aligned}$$

24.  $\gamma(E2)N \rightarrow N(\frac{5}{2}, 3) \rightarrow \sigma N$ :

$$\begin{aligned}\vec{L}^{(+)} &= -((p_1k) + (p_2k))([p_1\epsilon] + [p_2\epsilon]) - ((p_1\epsilon) + (p_2\epsilon))([p_1k] + [p_2k]), \quad \vec{L}^{(-)} = 0, \\ K^{(+)} &= 3[(p_1\epsilon) + (p_2\epsilon)][(p_1k) + (p_2k)], \quad K^{(-)} = 0, \\ A &= -\frac{1}{5} \frac{f_{N^*\sigma N} f_{\sigma\pi\pi}}{M_N m_\sigma} G_{N^*}(W) G_\sigma(w_{\pi\pi}).\end{aligned}$$

25.  $\gamma(M3)N \rightarrow N(\frac{5}{2}, 3) \rightarrow \sigma N$ :

$$\begin{aligned}\vec{L}^{(+)} &= k^2 \left[ 4((p_1k) + (p_2k))([p_1\epsilon] + [p_2\epsilon]) + ([p_1k] + [p_2k])((p_1\epsilon) + (p_2\epsilon)) \right. \\ &\quad \left. + \frac{3}{2}(\vec{p}_1 + \vec{p}_2)^2[k\epsilon] \right] - \frac{15}{2}[k\epsilon] [(p_1k) + (p_2k)]^2, \quad \vec{L}^{(-)} = 0, \\ K^{(\pm)} &= 0, \\ A &= \frac{1}{5\sqrt{7}} \frac{f_{N^*\sigma N} f_{\sigma\pi\pi}}{M_N^3 m_\sigma} G_{N^*}(W) G_\sigma(w_{\pi\pi}).\end{aligned}$$

- 
- [1] S. Capstic and W. Roberts, Phys. Rev. D **49**, 4570 (1994).  
[2] J.A. Gomez Tejedor and E. Oset, Nucl. Phys. A **600**, 413 (1996).  
[3] L.Y. Murphy and J.M. Laget, DAPHNIA/SPhN 96-10 (1996).  
[4] K. Ochi, M. Hirata, and T. Takaki, Phys. Rev. C **56**, 1472 (1997).  
[5] M. Ripani, V. Mokeev, M. Anghinolfi, *et al.*, Nucl.Phys. A **672**, 220 (2000).  
[6] D. Lüke and P. Söding, *Springer Tracts in Modern Physics* **59**, 39 (1971).  
[7] A. Zabrodin, G. Audit, R. Beck, *et al.*, Phys. Rev. C **55**, R1617 (1997).  
[8] V. Kleber, P. Achenbach, J. Ahrens, *et al.*, Eur. Phys. J. A **9**, 1 (2000).  
[9] J.D. Bjorken and S.D. Drell, *Relativistic Quantum Mechanics*, McGraw-Hill, 1964.  
[10] S. Ong and J. Wiele, Phys. Rev. C **63**, 024614 (2001).  
[11] Particle Data Group, Eur. Phys. J. C **15**, 1 (2000).  
[12] D. Drechsel, S.S. Kamalov, and L. Tiator, Nucl. Phys. A **645**, 145 (1999).  
[13] D.M. Manley, and E.M. Saleski, Phys. Rev. D **45**, 4002 (1992).  
[14] K. Gottfried and J.D. Jackson, Nuovo Cim. **33**, 309 (1964).  
[15] M.P. Locher and W. Sandhas, Z. Phys. **195**, 461 (1966).  
[16] A. Dar, Phys. Rev. Lett. **13**, 91 (1964).  
[17] M. Abramowitz and I.A. Stegun, *Handbook of Mathematical Functions*, National Bureau of Standards, 1972.  
[18] M.G. Hauser, Phys. Rev. **160**, 1215 (1967).  
[19] Aachen-Berlin-Bonn-Hamburg-Heidelberg-München Collaboration, Phys. Rev. **175**, 1669 (1968).  
[20] A. Braghieri *et al.*, Phys. Lett. B **363**, 46 (1995).  
[21] W. Langgärtner *et al.*, Phys. Rev. Lett. **87**, 052001 (2001).  
[22] M. Wolf *et al.*, Eur. Phys. J. A **9**, 5 (2000).  
[23] Y. Assafiri *et al.*, Phys. Rev. Lett. **90**, 222001 (2003).  
[24] J.C. Nacher, E. Oset, M.J. Vicente Vacas, and L. Roca, Nucl. Phys. A **695**, 295 (2001).  
[25] H.G. Hilpert *et al.*, Nucl. Phys. B **21**, 93 (1970).  
[26] Y. Oh and T.-S. H. Lee, Phys. Rev. C **69**, 025201 (2004).  
[27] H. Arenhövel, A. Fix, and M. Schwamb, Phys. Rev. Lett. **93**, 202301 (2004).  
[28] H.J. Arends, A2 collaboration, private communication.

- [29] L. Roca, E. Oset, and M.J. Vicente Vacas, Phys. Lett. B **541**, 77 (2002).
- [30] M. Hirata, N. Katagiri, and T. Takaki, Phys. Rev. C **67**, 034601 (2003).
- [31] F. Carbonara *et al.*, Nuov. Cim. **36A**, 219 (1976).
- [32] J.M. Laget, Phys. Rep. **69**, 1 (1981).
- [33] M.I. Levchuk, V.A. Petrunkin, and M. Schumacher, Z. Phys. A **355**, 317 (1996).
- [34] E.M. Darwish, H. Arenhövel, and M. Schwamb, Eur. Phys. J. A **16**, 111 (2003).
- [35] J. Haidenbauer and W. Plessas, Phys. Rev. C **30**, 1822 (1984).
- [36] V.M. Kolybasov, V.G. Ksenzov, Yad. Fiz. **22**, 720 (1975) (Sov. J. Nucl. Phys. **22**, 372 (1976)); U. Siodlaczek *et al.*, Eur. Phys. J. A **10**, 365 (2001).
- [37] R. Schiffer *et al.*, Nucl. Phys. B **38**, 628 (1972).
- [38] B. Krusche, M. Fuchs, V. Metag *et al.*, Eur. Phys. J. A **6**, 309 (1999).
- [39] M. Asai *et al.*, Z. Phys. A **344**, 335 (1995).
- [40] J.A. Gomez Tejedor, E. Oset, and H. Toki, Phys. Lett. B **346**, 240 (1995).
- [41] S. Strauch, Fizika **B 13**, 179 (2004), (nucl-ex/0407008).
- [42] G.F. Chew, M.L. Goldberger, F.E. Low, and Y. Nambu, Phys. Rev. **106**, 1345 (1957).

TABLE I: Listing of resonances included in the model. The partial decay widths are given in percent. The two values of  $\Gamma_{\pi\Delta}/\Gamma$  for  $D_{13} \rightarrow \pi\Delta$  and  $D_{33} \rightarrow \pi\Delta$  correspond to  $s$ - and  $d$ -wave  $\pi\Delta$  states. For  $S_{11}(1535)$  the partial  $\eta N$  decay width is equal to the  $\pi N$  width.

$L_2 T_2 J(M^*)$	M [MeV]	$\Gamma$ [MeV]	$\Gamma_{\pi N}/\Gamma$	$\Gamma_{\pi\Delta}/\Gamma$	$\Gamma_{\rho N}/\Gamma$	$\Gamma_{\sigma N}/\Gamma$	Multipoles
$P_{33}(1232)$	1232	120	100				E2, M1
$P_{11}(1440)$	1440	350	67	25		8	M1
$D_{13}(1520)$	1520	120	59	9, 12	20		E1, M2
$S_{11}(1535)$	1535	150	45		5	5	E1
$S_{31}(1620)$	1620	150	25	55	20		E1
$D_{15}(1675)$	1675	150	45	55			E3, M2
$F_{15}(1680)$	1680	130	69	10	9	12	E2, M3
$D_{33}(1700)$	1700	300	15	41, 4	40		E1, M2
$P_{13}(1720)$	1720	150	15		85		E2, M1

TABLE II: Listing of coupling constants for  $T = 1/2$  resonances. The signs of the hadronic constants are chosen according to  $\pi$  and  $\pi\pi$  production analyses as explained in Sect. II in the paragraph following Eq. (6). The two values for  $f_{N^*\pi\Delta}$  for  $D_{13}(1520)$  refer to  $s$ - and  $d$ -wave  $\pi\Delta$  states.

$L_2 T_2 J(M^*)$	$g^{E(s)}$	$g^{E(v)}$	$g^{M(s)}$	$g^{M(v)}$	$f_{N^*\pi N}$	$f_{N^*\pi\Delta}$	$f_{N^*\rho N}$	$f_{N^*\sigma N}$
$P_{11}(1440)$			0.089	0.375	-1.454	-4.219		-3.187
$D_{13}(1520)$	-0.015	0.236	0.640	0.915	-0.323	0.791, 0.846	7.651	
$S_{11}(1535)$	-0.053	-0.163			-1.219		3.842	-3.851
$D_{15}(1670)$	-0.032	-0.052	-0.227	0.443	-0.196	-0.706		
$F_{15}(1680)$	0.202	0.248	0.510	1.452	-0.082	0.458	7.888	-6.572
$P_{13}(1720)$	-0.109	-0.026	-0.067	0.036	0.269		18.840	

TABLE III: Same as in Table II for  $T = 3/2$  resonances.

$L_2 T_2 J(M^*)$	$g^E$	$g^M$	$f_{N^*\pi N}$	$f_{N^*\pi\Delta}$	$f_{N^*\rho N}$
$P_{33}(1232)$	-0.087	-1.845	2.230	2.982	
$S_{31}(1620)$	-0.069		0.879	1.068	-4.067
$D_{33}(1700)$	0.236	-0.506	0.149	2.008, 0.237	4.417

TABLE IV: Listing of hadronic vertices  $F_{N^*(J,L) \rightarrow X}$ . The empty spaces in the last two columns indicate that the corresponding couplings are insignificant or not provided by the PDG compilation [11] for the resonances of the model.

$J, L$	$X = \pi N$	$\pi \Delta$	$\rho N$	$\sigma N$
$\frac{1}{2}, 0$	$-i f_{N^* \pi N}$	$-i \frac{f_{N^* \pi \Delta}}{m_\pi^2} (\sigma_{\frac{3}{2}, \frac{1}{2}}^{[2]} \cdot q^{[2]})$	$f_{N^* \rho N} (\sigma_{\frac{1}{2}, \frac{1}{2}}^{[1]} \cdot \epsilon_\rho^{[1]})$	$\frac{f_{N^* \sigma N}}{m_\sigma} (\sigma_{\frac{1}{2}, \frac{1}{2}}^{[1]} \cdot q^{[1]})$
$\frac{1}{2}, 1$	$-i \frac{f_{N^* \pi N}}{m_\pi} (\sigma_{\frac{1}{2}, \frac{1}{2}}^{[1]} \cdot q^{[1]})$	$-i \frac{f_{N^* \pi \Delta}}{m_\pi} (\sigma_{\frac{3}{2}, \frac{1}{2}}^{[1]} \cdot q^{[1]})$		$f_{N^* \sigma N}$
$\frac{3}{2}, 1$	$-i \frac{f_{N^* \pi N}}{m_\pi} (\sigma_{\frac{1}{2}, \frac{3}{2}}^{[1]} \cdot q^{[1]})$	$-i \frac{f_{N^* \pi \Delta}}{m_\pi} (\sigma_{\frac{3}{2}, \frac{3}{2}}^{[1]} \cdot q^{[1]})$	$\frac{f_{N^* \rho N}}{m_\rho} (\sigma_{\frac{1}{2}, \frac{3}{2}}^{[1]} \cdot [q^{[1]} \otimes \epsilon_\rho^{[1]}]^{[1]})$	
$\frac{3}{2}, 2$	$-i \frac{f_{N^* \pi N}}{m_\pi^2} (\sigma_{\frac{1}{2}, \frac{3}{2}}^{[2]} \cdot q^{[2]})$	$-i f_{N^* \pi \Delta} - i \frac{f_{N^* \pi \Delta}^{(d)}}{m_\pi^2} (\sigma_{\frac{3}{2}, \frac{3}{2}}^{[2]} \cdot q^{[2]})$	$f_{N^* \rho N} (\sigma_{\frac{1}{2}, \frac{3}{2}}^{[1]} \cdot \epsilon_\rho^{[1]})$	
$\frac{5}{2}, 2$	$-i \frac{f_{N^* \pi N}}{m_\pi^2} (\sigma_{\frac{1}{2}, \frac{5}{2}}^{[2]} \cdot q^{[2]})$	$-i \frac{f_{N^* \pi \Delta}}{m_\pi^2} (\sigma_{\frac{3}{2}, \frac{5}{2}}^{[2]} \cdot q^{[2]})$		
$\frac{5}{2}, 3$	$-i \frac{f_{N^* \pi N}}{m_\pi^2} (\sigma_{\frac{1}{2}, \frac{5}{2}}^{[3]} \cdot q^{[3]})$	$-i \frac{f_{N^* \pi \Delta}}{m_\pi} (\sigma_{\frac{3}{2}, \frac{5}{2}}^{[1]} \cdot q^{[1]})$	$\frac{f_{N^* \rho N}}{m_\rho} (\sigma_{\frac{1}{2}, \frac{5}{2}}^{[2]} \cdot [q^{[1]} \otimes \epsilon_\rho^{[1]}]^{[2]})$	$\frac{f_{N^* \sigma N}}{m_\sigma^2} (\sigma_{\frac{1}{2}, \frac{5}{2}}^{[2]} \cdot q^{[2]})$

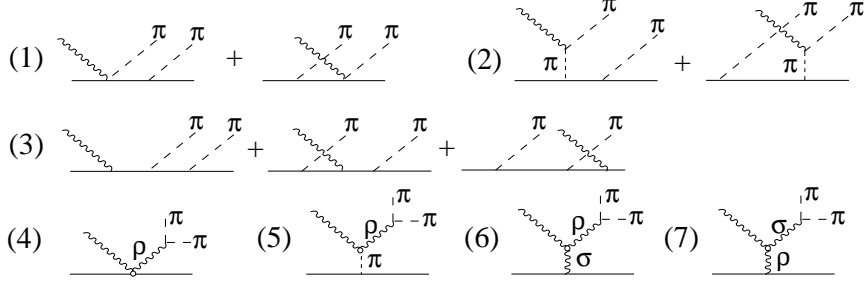
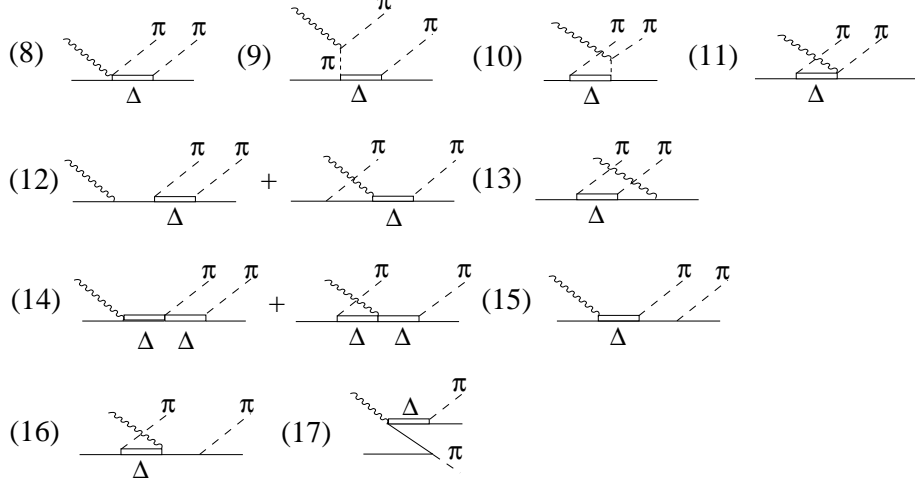
TABLE V: Isospin coefficients  $C_l^{(\pm)}$  (A.12) for the resonance amplitudes. The isospin of a resonance is indicated in parenthesis. The coefficients contain electromagnetic coupling constants  $g$  introduced in (B.9). For the resonances with isospin 1/2 they are split into isoscalar  $g^{(s)}$  and isovector  $g^{(v)}$  parts. In the lower part we give the corresponding coefficients for several important Born amplitudes where the associated diagram is indicated in parenthesis.

	$C_1^{(+)}$	$C_2^{(+)}$	$C_3^{(+)}$	$C_1^{(-)}$	$C_2^{(-)}$	$C_3^{(-)}$
$\gamma N \rightarrow N^*(1/2) \rightarrow \pi \Delta$	$-\frac{2\sqrt{2}}{3} g^{(s)}$	$-\frac{2\sqrt{2}}{3} g^{(v)}$		$\frac{\sqrt{2}}{3} g^{(s)}$	$-\frac{\sqrt{2}}{3} g^{(v)}$	$-\frac{2\sqrt{2}}{3} g^{(v)}$
$\gamma N \rightarrow N^*(1/2) \rightarrow \rho N$				$\frac{1}{\sqrt{3}} g^{(s)}$	$-\frac{1}{\sqrt{3}} g^{(v)}$	$-\frac{2}{\sqrt{3}} g^{(v)}$
$\gamma N \rightarrow N^*(1/2) \rightarrow \sigma N$	$-\sqrt{\frac{2}{3}} g^{(s)}$	$-\sqrt{\frac{2}{3}} g^{(v)}$				
$\gamma N \rightarrow N^*(3/2) \rightarrow \pi \Delta$		$-\frac{2}{3\sqrt{10}} g$	$\frac{2}{\sqrt{10}} g$		$-\frac{\sqrt{10}}{3} g$	$\frac{\sqrt{10}}{3} g$
$\gamma N \rightarrow N^*(3/2) \rightarrow \rho N$					$-\sqrt{\frac{2}{3}} g$	$\sqrt{\frac{2}{3}} g$
$\Delta$ -KR (8)		$-\frac{2}{3}$	$\frac{2}{3}$		$-\frac{4}{3}$	$\frac{2}{3}$
$N\Delta$ ( $u$ -channel) (2nd of 12)		$\sqrt{\frac{2}{3}}$	$\sqrt{\frac{2}{3}}$		$-\sqrt{\frac{2}{3}}$	$\sqrt{6}$
$\Delta\Delta$ ( $u$ -channel) (2nd of 14)	$\frac{2}{3}$	$\frac{4}{3}$	$-\frac{2}{3}$	$-\frac{1}{3}$	$\frac{5}{3}$	
$\rho$ -KR (4)						$-2$
$\gamma \rightarrow \rho$ ( $\sigma$ -exchange) (6)					$-1$	

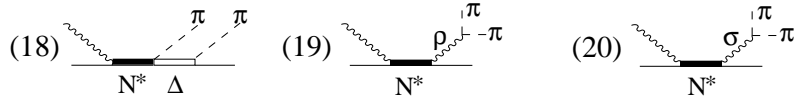
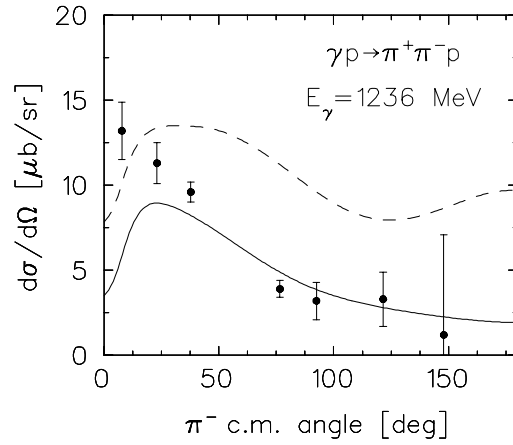
TABLE VI: Contribution of individual charge channels of double pion photoproduction on nucleon and deuteron to the finite GDH integral (in  $\mu\text{b}$ ), evaluated up to 1.5 GeV. The last column comprises the total finite GDH integral from  $\pi$ ,  $\eta$ , and  $\pi\pi$  photoproduction and in case of the deuteron from photodisintegration.

	$\pi^+ \pi^-$	$\pi^0 \pi^0$	$\pi^+ \pi^0$	$\pi^- \pi^0$	$\Sigma \pi\pi$	total [ $\mu\text{b}$ ]
neutron	22.23	1.82	33.28		57.33	190.51
proton	16.36	1.60		31.01	48.97	216.58
deuteron	43.16	3.53	29.46	27.98	104.13	-27.90

## N-BORN TERMS

 $\Delta$ -BORN TERMS

## RESONANCE TERMS

FIG. 1: Diagrams for the reaction  $\gamma N \rightarrow \pi\pi N$  used in the present work.FIG. 2:  $\pi^-$  angular distribution for  $\gamma N \rightarrow \pi^- \pi^+ p$ . The solid (dashed) curves are calculated with (without) absorption correction. The data are taken from Ref. [18].

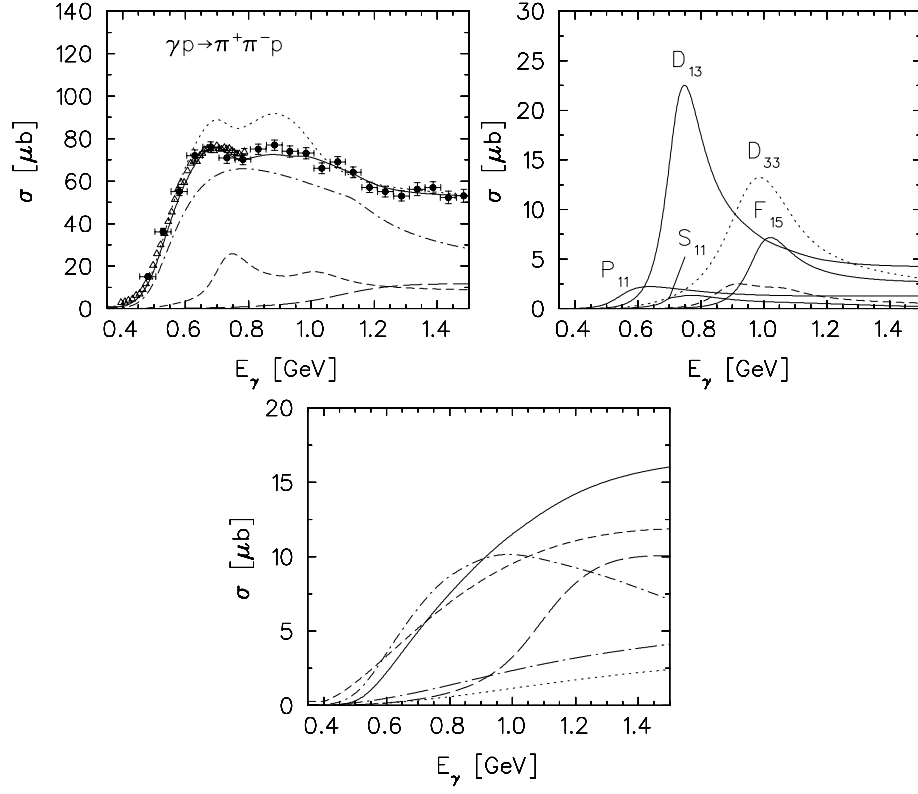


FIG. 3: Total cross section for  $\gamma p \rightarrow \pi^+ \pi^- p$ . Contributions of individual diagrams as follows: Upper left panel: dash-dotted:  $\Delta$  Kroll-Ruderman term plus pion-pole term (diagrams (8) and (9)); short dashed: all resonance terms (diagrams (18),(19) and (20)); long dashed:  $\rho^0$ -photoproduction via  $\pi^0$  and  $\sigma$ -exchange (diagrams (5) and (6)); solid: resulting cross section without  $D_{33}(1700)$ ; dotted: additional inclusion of  $D_{33}(1700)$ . The data are from Ref. [19] (circles) and Ref. [20] (triangles). Upper right panel: solid: contributions of  $P_{11}(1440)$ ,  $D_{13}(1520)$ ,  $F_{15}(1680)$ , and  $S_{11}(1535)$ ; dotted: contribution of  $D_{33}(1700)$ ; dashed: combined contribution of  $S_{31}(1620)$ ,  $P_{13}(1720)$ , and  $D_{15}(1675)$ . Lower panel: solid: contribution of diagrams (12); short-dashed: diagrams (1) and (2); long-dashed: diagram (6); short dash-dotted: diagrams (14); dotted: diagrams (3); long-dash-dotted: remaining Born terms.

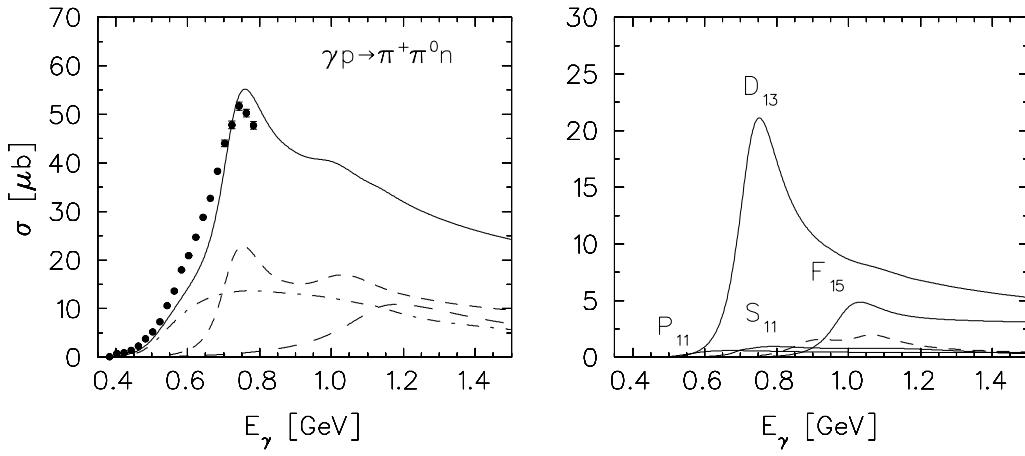


FIG. 4: Same as in Fig. 3 for  $\gamma p \rightarrow \pi^+ \pi^0 n$ . Long-dashed line on the left panel is the contribution of the nonresonant  $\rho^+$ -photoproduction (contact term (4) and  $\pi$ -exchange term (5)). The data are from Ref. [21].



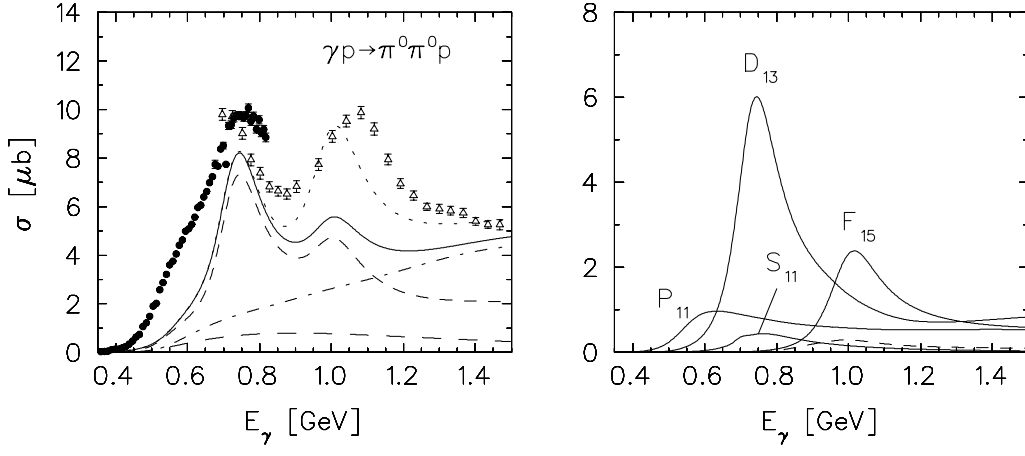


FIG. 5: Total cross section for  $\gamma p \rightarrow \pi^0 \pi^0 p$ . Left panel: dash-dotted: contribution of  $N\Delta$   $s$ - and  $u$ -channels (diagrams (12)); long-dashed: contribution of the  $Z$ -graph (diagram (17)); dotted: calculation with positive sign of the  $F_{15}(1680) \rightarrow \pi\Delta$  amplitude as predicted in [1]. Experimental data from Ref. [22] (circles) and Ref. [23] (triangles). Right panel: solid: contributions of  $P_{11}(1440)$ ,  $D_{13}(1520)$ ,  $F_{15}(1680)$ , and  $S_{11}(1535)$ ; dotted: contribution of  $D_{33}(1700)$ ; dashed: combined contribution of  $S_{31}(1620)$ ,  $P_{13}(1720)$ , and  $D_{15}(1675)$ .

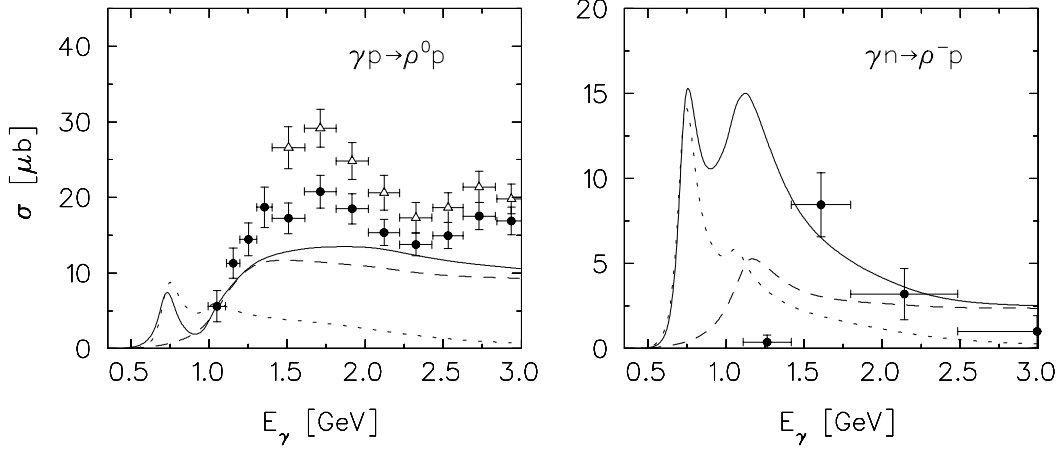


FIG. 6: Total cross sections for  $\rho$  photoproduction. Dotted curves: contribution from baryonic resonances in the  $s$ -channel. Left panel: dashed curve: contribution of  $\sigma$ -exchange (diagram (6)). Experimental data from Ref. [19]. Right panel: dashed curve: contact term (4). Experimental data from Ref. [25].

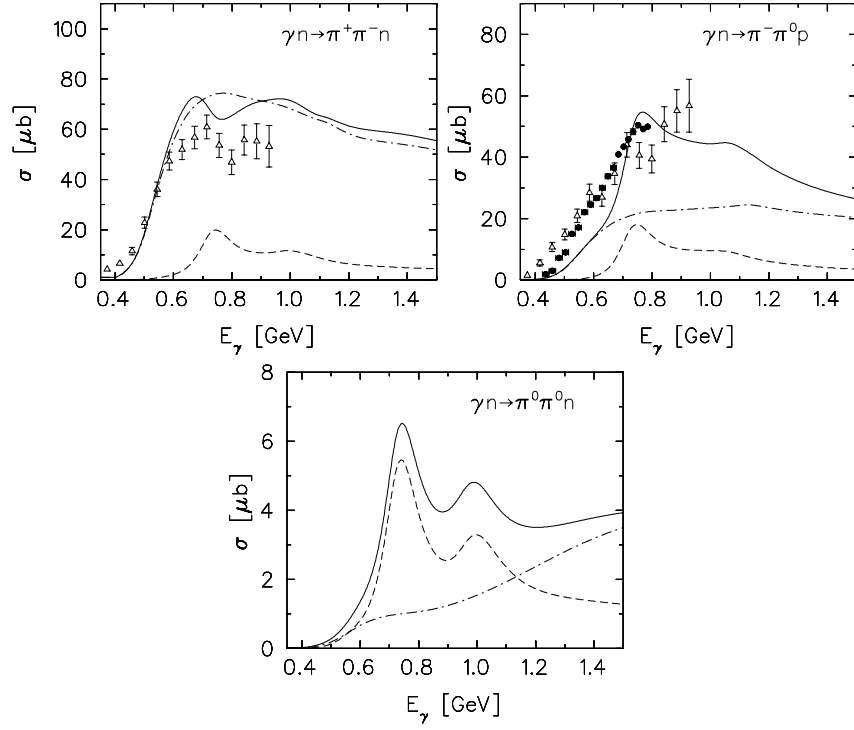


FIG. 7: Total cross section for double pion photoproduction on the neutron for different charge channels. Dashed curves: only resonance diagrams; dash-dotted curves: Born diagrams alone. Experimental data from Ref. [31] (triangles) and Ref. [7] (circles).

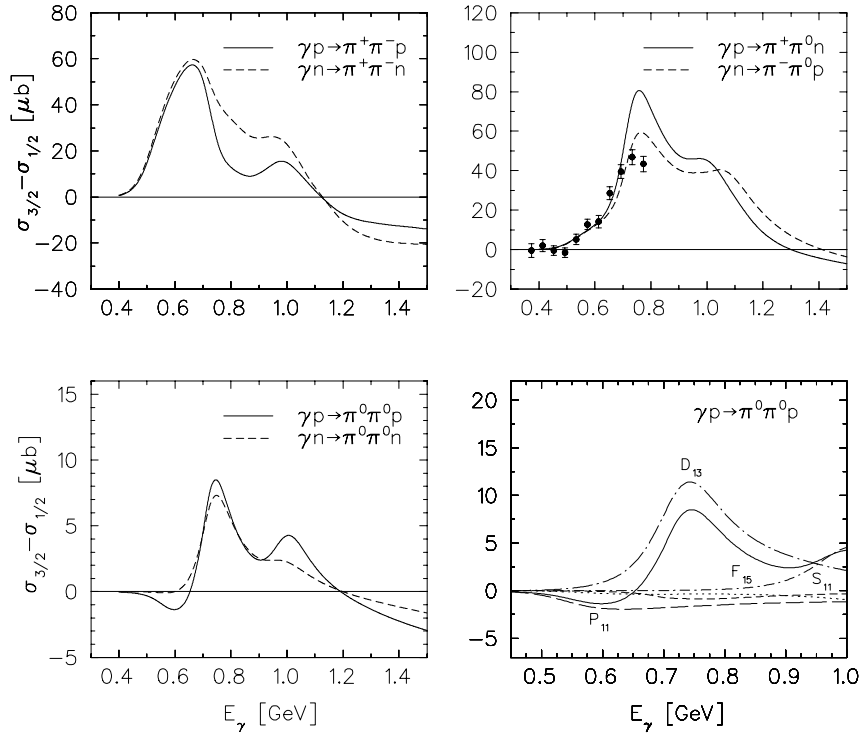


FIG. 8: Helicity asymmetry  $\sigma_{3/2} - \sigma_{1/2}$  (15) for  $\gamma N \rightarrow \pi\pi N$  in different charge channels. Lower right panel: individual contributions of  $P_{11}$ (1440),  $D_{13}$ (1520),  $S_{11}$ (1535), and  $F_{15}$ (1680) resonances. Dotted curve represents the combined contribution of Born diagrams and the solid curve the total asymmetry.

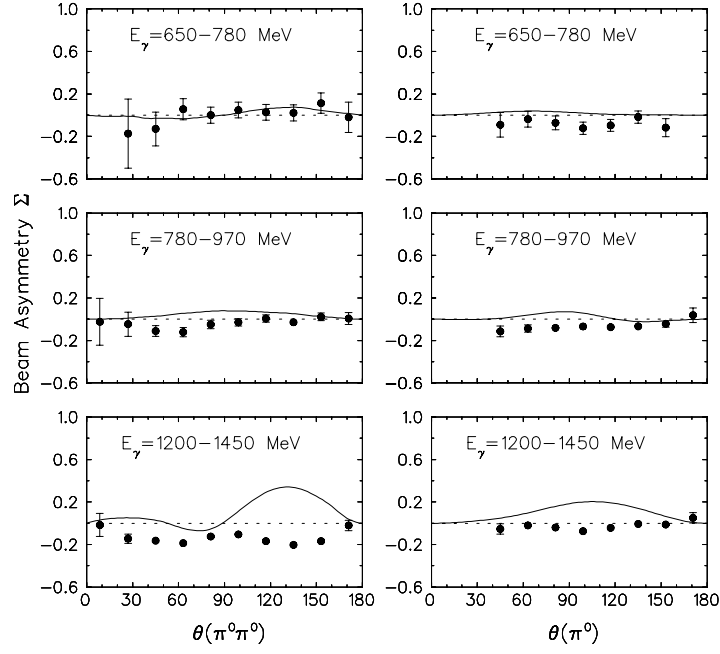


FIG. 9: Beam asymmetry  $\Sigma$  for linearly polarized photons for  $\gamma p \rightarrow \pi^0 \pi^0 p$ . On the left panels  $\theta(\pi^0 \pi^0)$  denotes the angle of the total two-pion momentum, and on the right panels  $\theta(\pi^0)$  refers to the angle of one of the produced pions. The data are from Ref. [23].

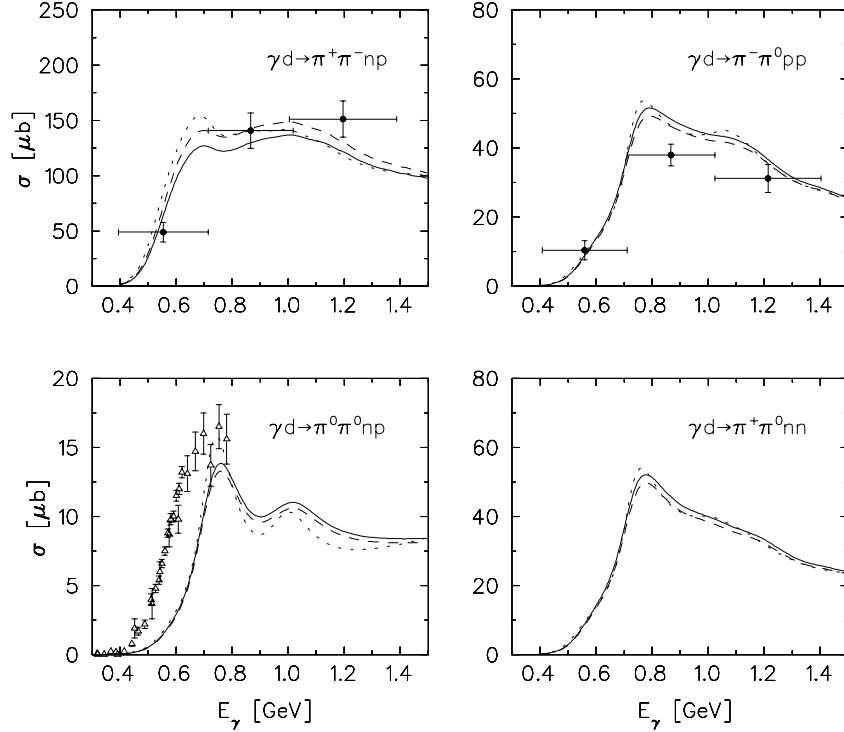


FIG. 10: Total cross section for incoherent double pion photoproduction on a deuteron for different charge channels. Solid and dashed curves are obtained with and without final  $NN$  interaction. Dotted curves show the corresponding elementary cross sections. In  $\pi^+\pi^-$  and  $\pi^0\pi^0$  channels they are calculated as a sum of the cross sections on a proton and a neutron. The data are from Ref. [37] (circles) and Ref. [38] (triangles).

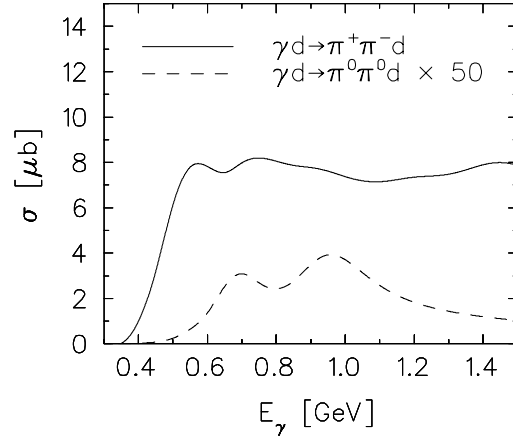


FIG. 11: Total cross sections for coherent double pion photoproduction on a deuteron. The solid and the dashed curves represent the  $\pi^+\pi^-$  and  $\pi^0\pi^0$  channels, respectively. The  $\pi^0\pi^0$  cross section is multiplied by a factor 50.

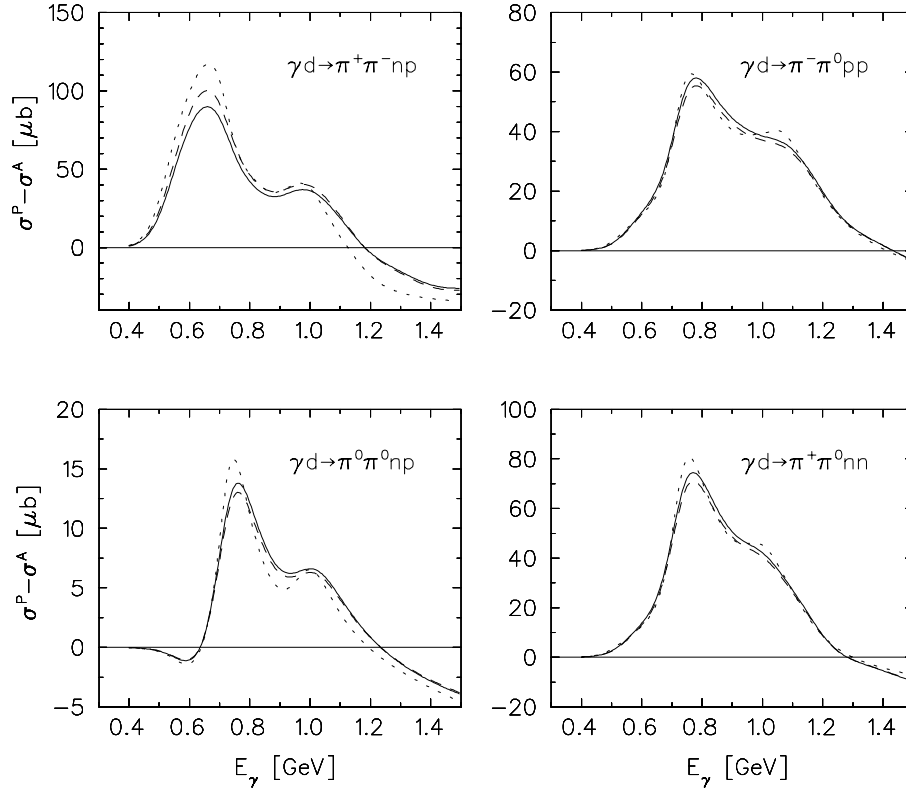


FIG. 12: Helicity asymmetry for incoherent double pion photoproduction on a deuteron. The notation of the curves is as in Fig. 10.